ACS APPLIED BIO MATERIALS

www.acsabm.org

Review

Recent Progress on Transparent Microelectrode-Based Soft Bioelectronic Devices for Neuroscience and Cardiac Research

Luyao Lu*

Cite This: *ACS Appl. Bio Mater.* 2023, 6, 1701−1719

Read Online

ACCESS | Metrics & More | Article Recommendations

ABSTRACT: Transparent microelectrodes have emerged as promising tools to combine electrical and optical sensing and modulation modalities in many areas of biological and biomedical research. Compared to conventional opaque microelectrodes, they offer a number of specific advantages that can enable advances in functionality and performance. In addition to optical transparency, the mechanical softness feature is desired to minimize foreign body responses, increase biocompatibility, and avoid loss of functionality. In this review, we present recent research from the past several years on transparent microelectrode-based soft bioelectronic devices with an emphasis on their material properties and advanced device designs, as well as multimodal application scenarios for neuroscience and cardiology. First, we introduce material candidates with proper electrical, optical, and mechanical properties for soft transparent microelectrodes. We then discuss examples of soft transparent microelectrode arrays tailored to combine electrical recording and/or stimulation with optical imaging and/or optogenetic modulation of the brain and the heart. Next, we summarize the most recent progress on soft opto-electric devices integrating transparent microelectrodes with microscale light-emitting diodes and/or photodetectors into single and hybrid microsystems as powerful tools to explore the brain and heart functions. A brief overview of possible future directions of soft transparent microelectrode-based biointerfaces is provided to conclude the review.

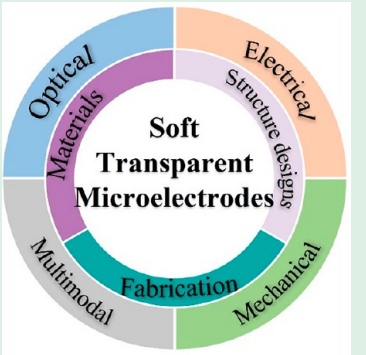

KEYWORDS: *transparent microelectrodes, flexible electronics, cardiac interface, neural interface, LEDs, photodetectors*

1. INTRODUCTION

Studying the functions of cells and tissues to understand the complex physiology of some of the most vital organs such as the brain and heart in health and disease represents an important research area for biological and biomedical sciences. Successful outcomes will not only contribute to our knowledge of the (patho)physiological function of brain and heart systems, but also greatly facilitate the development of treatment methodologies for neurological disorders and cardiovascular diseases. In this context, a significant research effort focuses on developing advanced electrical and optical interfaces to interact with various parts of these organs.[1−5] For example, microelectrodes are one of the most widely applied tools to record action potentials and local field potentials with high temporal resolution from the brain and heart to reflect their physiological states and monitoring health status.[6−8] Direct microelectrode-based electrical stimulations, such as cardiac pacing[9−11] and deep brain stimulation,[12,13] are clinically used to treat arrhythmias and Parkinson's disease by triggering an action potential with an external current and changing the membrane potential. Despite the tremendous impact of microelectrode-based electrical recording and stimulation approaches on fundamental research and translational development, they have limited spatial resolution, which is crucial to differentiate cell types, shapes, and understand the complicated network connections. They are also problematic in directly probing important functional physiological parameters such as metabolic activity, intracellular calcium dynamics, or target specific cell types.[14] Optical techniques, such as optogenetics[15−17] and optical imaging,[18−20] can provide cell-type specificity and high spatial resolution to either manipulate or monitor cells via light-sensitive proteins (opsins) and fluorescent reporters. Those optical methods have now been widely applied to rodents, worms, fish, and nonhuman primates for investigating basic physiology and disease mechanisms. However, their temporal resolution is limited by the dynamics of the opsins and fluorescent reporters used. In addition to improving platforms for separate electrical and optical studies, combining different methodologies is an important trend in technology development because this will leverage the advantages while compensating for the weaknesses of individual approaches. Although there has been tremendous progress in microsystem platforms integrating electrical and optical components,[21,22] a precise correlation of electrical signals

Received: February 16, 2023
Accepted: April 7, 2023
Published: April 20, 2023

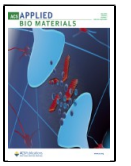

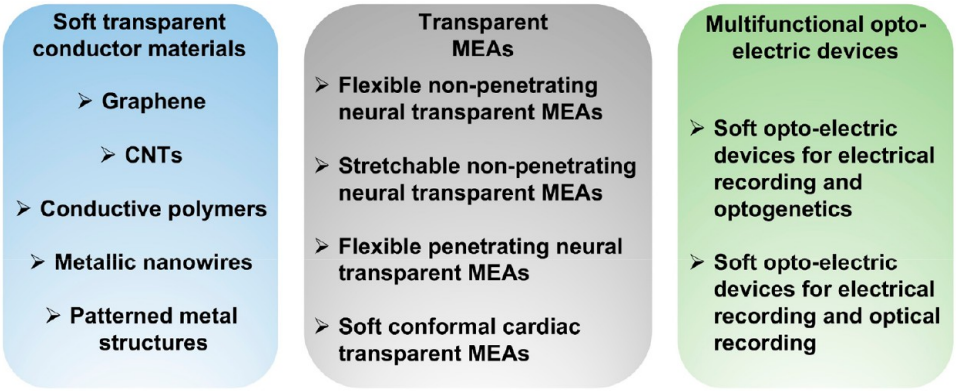

Figure 1. Overall scheme of soft transparent microelectrode materials, soft MEAs, multimodal bioelectronic devices, and their applications in neuroscience and cardiology discussed in this review.

with optical imaging data or optical modulation is difficult. This is because conventional microelectrodes rely on opaque conductors and prevent simultaneous colocalized electrical and optical interfacing due to complications such as photoelectric artifacts and obscured fields of view for light delivery to or collection from areas underneath the microelectrodes.[23] The photoelectric artifacts here refer to the electrical noises in the microelectrode recorded signals from the interaction between microelectrodes and photons that generates the potential differences and surface current flows.[24]

Soft optically transparent microelectrodes are critical technologies that can conformally integrate with tissues and allow light to transmit through the microelectrodes in both directions for colocalized electrophysiology, optogenetics, and optical imaging with minimal photoelectric artifacts. Over the past decade, tremendous progress in advanced materials, unusual mechanics design, and microfabrication methods has generated many types of soft transparent microelectrodes from various low modulus materials and structures with comparable electrochemical performance to conventional opaque microelectrodes for neuroscience and cardiac research. For example, carbon-based nanomaterials,[25,26] conductive polymers,[27] and metal nanowires[28] could directly serve as intrinsically soft transparent microelectrode materials. Patterned porous structures from opaque conductors such as metal grid/mesh also generate microelectrodes with a high optical transparency.[29,30] Hybrid composite materials further improve the chemical, electrical, and optical performances of the resulting transparent microelectrodes.[31−33]

In this review, we discuss the latest advances in transparent microelectrode-based soft neural and cardiac interfaces from materials, device design, and integration, *ex vivo* and *in vivo* application perspectives (Figure 1). A variety of materials and structure designs for transparent microelectrode applications with excellent optical transparency, high conductivity, low electrochemical impedance, high charge storage capacity (CSC), and reduced mechanical mismatch between the electronics and biological tissues to record/stimulate electrical signals with high signal-to-noise ratios (SNRs) are introduced first. Then, we highlight flexible and stretchable transparent microelectrode arrays (MEAs) from those materials and their combinations with optical modalities for neuroscience and cardiac research. Those MEAs are typically deposited and patterned on the surfaces of soft transparent plastic substrates, including (i) flexible polymers, such as polyethylene terephthalate (PET) and parylene-C, to enable the direct development of functional components through conventional microfabrication processes and (ii) stretchable elastomers, such as polydimethylsiloxane (PDMS), to further reduce the mechanical mismatch at the device/tissue interface and enable device operations under mechanically active environment. Tissue-like mechanics are desired for the MEAs to not only improve the quality of the collected signals from three-dimensional (3D) complex organ structures but to also reduce the foreign body responses around the MEAs. Following that, recent breakthroughs in directly integrating transparent microelectrodes with microscale light-emitting diodes (μ-LEDs) and microscale photodetectors (μ-PDs) into hybrid "all in one" microsystems for multimodal investigations with a single device platform are described. Typical fabrication approaches used in transparent microelectrode-based soft bioelectronic devices, including solution processes (e.g., spin coating), lithography, chemical etching, evaporation, transfer printing, etc. are discussed in different sections. At the end of this review, we discuss the opportunities for future transparent microelectrode-based biointerfaces for biomedical engineering and medical applications.

2. CONDUCTOR MATERIALS AND STRUCTURES FOR TRANSPARENT MICROELECTRODES

Transparent conductors are the basis for the construction of soft transparent microelectrodes. The conductors will transmit bioelectrical signals from electrogenic cells through electrical couplings between the microelectrodes and cells with high fidelity. When used as interconnects for the microelectrodes, the conductors will transmit the bioelectrical signals with minimal signal attenuation to the external data acquisition systems. As a result, the conductive materials largely determine the electrochemical, optical, and electrical performances of the devices. In the following section, we present conductive materials and structures for soft transparent microelectrodes, including graphene, carbon nanotubes (CNTs), conductive polymers, metallic nanowires, and patterned metal structures. Some other emerging conductive materials (e.g., graphdiyne, MXene) that have not been used in transparent microelectrode-based electrophysiological studies are not included, and we refer the readers to other recent review papers on these materials.[34−36]

2.1. Graphene. Graphene is a two-dimensional (2D) carbon allotrope with a single layer sheet of sp^2 hybrid carbon atoms in a hexagonal structure. Due to its ultrathin nature, monolayer graphene only absorbs ~2.3% of visible light and shows a high visible optical transmittance of >97% with a negligible

https://doi.org/10.1021/acsabm.3c00131
ACS Appl. Bio Mater. 2023, 6, 1701−1719

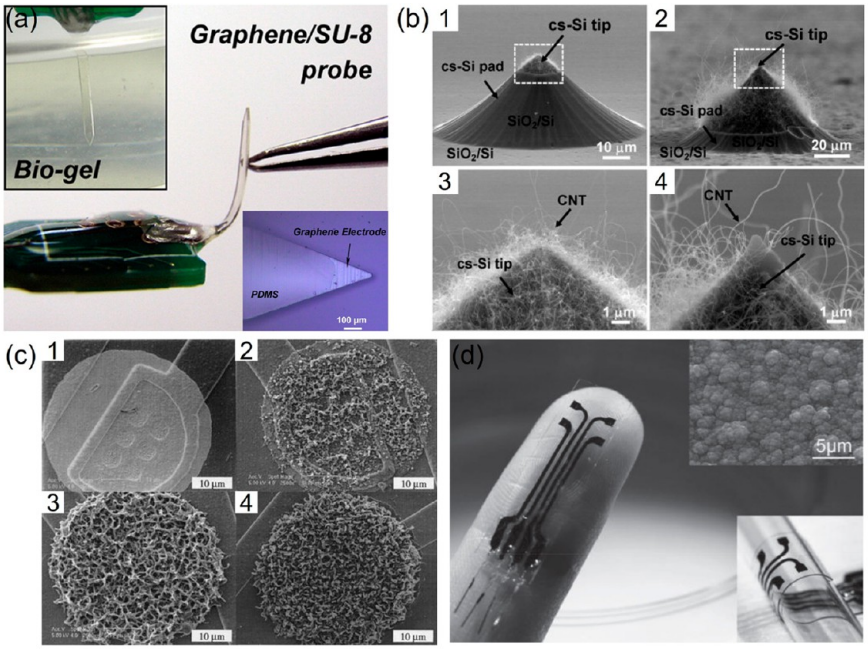

Figure 2. Carbon-based transparent microelectrode materials. (a) Photos of a flexible graphene microprobe penetrating in an agar gel (top left) and after 90° bending (middle). Microscopic image of the exposed graphene area at the tip of microprobe (bottom right). Reproduced from ref 49. Copyright 2013, Elsevier. (b) Scanning electron microscopy (SEM) images of the cone-shaped tips of CNT probes with sizes of (1) 16 μm and (2) 65 μm. The (3) and (4) show magnified SEM images of the highlighted areas of (1) and (2), respectively. Reproduced from ref 71. Copyright 2010, Elsevier. (c) SEM images (1−4) of PPy-coated electrodes deposited with 0, 1, 4, and 10 μC of charge. Reproduced from ref 83. Copyright 2001, Wiley. (d) Conductive polymer PPy/polycaprolactone-*block*-polytetrahydrofuran-*block*-polycaprolactone microelectrodes formed on an elastomer substrate. (Top right) SEM image of the microelectrode surface. (Bottom right) A MEA conformably wrapped around a glass pipet. Reproduced from ref 87. Copyright 2014, Wiley.

reflectance of ∼0.1%.[37−39] In addition, ultrathin 2D graphene shows excellent mechanical flexibility and strength, resulting from the atomic thickness and strong in-plane covalent bonding between carbon atoms. For example, graphene can endure 4% strain with negligible cracking. The measured Young's modulus and breaking strength of graphene are as high as 1.0 TPa and 42 N/m, respectively.[40] The sp^2 hybridization and delocalization of π electrons lead to an electron mobility of 106 S/m and a sheet resistance (R_{sh}) from several tens to 100 Ω/sq, respectively.[41,42] Due to its appealing physicochemical properties, graphene has been widely used by the scientific community in electrical recording/stimulation applications.[43−45] For example, it could be integrated on a PET film as a flexible, transparent, and biocompatible stimulation electrode for cultured neural cells.[46] The optical transparency of the graphene/PET electrodes allows simultaneous optical examination of the morphological changes from the cells in relation to electrical stimulation. The results showed that weak electric field stimulation as low as 4.5 mV/mm could promote cell-to-cell interaction. Graphene microelectrodes could further serve as contact lens electrodes for electroretinography measurements due to their optical transparency and softness.[47] Meanwhile, it should be noted that graphene is not completely free of photoelectric artifacts, and multilayer stacked graphene devices could serve as biointerfaces to efficiently convert light into electricity to achieve light-controlled cellular stimulation.[48] The electrochemical performance of graphene microelectrodes can be improved by chemical treatments such as plasma treatment,[49] doping,[50] and surface modifications.[51,52] Chen et al. designed a flexible graphene microprobe for neural and cardiac recording in crayfish and zebrafish (Figure 2a).[49] The graphene-coated SU-8 substrates were treated by steam plasma to change the surface from hydrophobic to hydrophilic and reduce the impedance, which increased the SNR of the measured action potentials from 20.3 ± 3.3 to 27.8 ± 4.0 dB. Lu et al. developed transparent graphene microelectrodes with reduced impedance by electrodeposition of platinum (Pt) nanoparticles on graphene surfaces.[52] The resulting microelectrodes were able to exceed the quantum capacitance limit and lower the impedance 100 times, though at the cost of a decreased optical transparency (from >90% in monolayer graphene to ∼50% after 30 s electrodeposition). Electroplating conductive polymer poly(3,4-ethylenedioxythiophene):polystyrenesulfonate (PEDOT:PSS) on graphene surface also improved its electrochemical performance.[32] The 1 kHz electrochemical impedance value serves as a benchmark for comparing the electrical recording performance of different microelectrodes. Low impedance values are desired for high-fidelity electrical recording. The optical transparency and 1 kHz impedance of the PEDOT:PSS-coated graphene microelectrodes could be tuned from ∼90% and 700 kΩ to ∼50% and 42 kΩ, respectively.

2.2. CNTs. CNTs are highly conductive one-dimensional (1D) carbon-based materials with cylindrical structures. CNTs are made of rolled-up graphene sheets and are categorized as either single-walled CNTs (SWCNTs) or multiwalled CNTs (MWCNTs) based on the number of graphene sheets.[53,54] SWCNTs can behave as a metal or semiconductor depending on their diameter and chirality. The maximum theoretical conductivity of a SWCNT network is ∼90,000 S/cm, corresponding to a R_{sh} of 10 Ω/sq and an optical transmittance of 92%.[55] The Young's modulus of SWCNT composites is between 0.65 and 5.5 TPa.[56] MWCNTs commonly show lower

https://doi.org/10.1021/acsabm.3c00131
ACS Appl. Bio Mater. 2023, 6, 1701−1719

conductivity than those from SWCNTs because the inner walls in MWCNTs may act as noncurrent carrying voids in the network.[57,58] In addition, SWCNT-based electrodes have better optical properties than MWCNT-based electrodes under the same conditions since a greater amount of light will be absorbed when the number of walls in the individual CNTs increases.[59] Wong et al. demonstrated that MWCNTs exhibited an average Young's modulus of 1.28 TPa and an average bending strength of 14 GPa.[60] Importantly, CNTs can form a thin conductive network that is mechanically flexible or even stretchable and optically transparent resulting from the intersliding behavior and the void space between the interconnected CNTs in the network.[59,61,62] When mixed with polymers, the type of polymer matrix and the aspect ratio of CNTs also significantly influence the elastic modulus.[63] The physical properties of CNT networks can be adjusted by individual nanotubes (e.g., changing their chirality, diameter, length, doping level, etc.) and their geometry in the network (e.g., varying CNT density, layer thickness, alignment among nanotubes, etc.). In general, a thinner nanotube diameter improves the optical transparency while longer nanotubes result in higher conductivity.[64] Advances of CNT synthesis, purification, and surface functionalization methods have opened pathways for CNTs as high-performance biocompatible components for biosensors and implant coatings,[65−67] due to their high specific surface areas (700−1,000 m^2/g), low impedance, and high charge transfer characteristics.[68−70] For example, Keefer et al. applied MWCNTs to improve the interface between indium tin oxide (ITO), tungsten, stainless steel wire electrodes, and the surrounding tissue.[69] The 1 kHz impedance decreased from 940 to 38 kΩ while an approximately 40-fold increase in charge transfer capability was observed after coating CNTs. Su et al. demonstrated low impedance CNT-based microelectrodes with a miniature diameter at 3.5 μm for high resolution electrical recording by growing CNTs on cone-shaped silicon probes with a large surface area (Figure 2b).[71] The resulting microelectrodes exhibited a low impedance per unit area at ∼64.5 Ω/mm^2 and a specific capacitance at ∼2.5 mF/cm^2. Chen et al. tested the biocompatibility of CNTs by comparing the health of rat hippocampal neurons cultured on CNT MEAs to that on a glass substrate for 16 days.[72] The resulting neuron density and morphology on the CNT MEAs were comparable to the control glass, confirming the excellent biocompatibility.

2.3. Conductive Polymers. The electrical signals in biological systems such as nervous systems are controlled by neurotransmitter diffusion between synapses and ionic transport across cell membranes. Therefore, microelectrodes that can accommodate both ionic and electronic transport are of particular interest for interfacing with biology. In this context, conductive polymers have recently gained much attention due to their combined ionic−electronic conductivity, superior mechanical properties, and biocompatibility.[73−76] Conductive polymers are also carbon-based materials and have alternating single and double bond structures to provide high conductivity after suitable doping. They normally have much lower Young's modulus than metals (∼1 GPa vs >100 GPa), which is beneficial to reduce the mechanical mismatch at the device and tissue interfaces.[77,78] Promising conductive polymers such as polypyrrole (PPy), PEDOT, and some of their derivatives were initially used as surface coating materials for conventional metal microelectrodes via electrochemical polymerization to optimize the microelectrode performance.[79−83] In one study, Cui et al. modified the surface of neural microelectrodes with proteins and PPy.[83] Figure 2c shows the morphologies of the resulting microelectrodes, which were rough and fuzzy to provide a high surface area and low impedance for interaction with neurons. More recently, flexible microelectrodes using conductive polymers as the sole conductor have been developed to avoid the problems with metal parts, such as high mechanical rigidity and potential for delamination.[84−86] Guo et al. prepared the first stretchable nerve MEA using conductive polymer PPy/polyolborate composites as the sole conductor for both the microelectrodes and interconnects (Figure 2d).[87] The MEA could withstand up to 23% uniaxial tensile strain with negligible changes in electrical conductivity. In addition, the microelectrodes exhibited a high CSC of 48.8 mC/cm^2, which was even better than commonly used stimulation microelectrode materials, such as Pt and iridium oxide (IrO_x). The higher CSC values are beneficial for electrical stimulation applications. Chen and co-workers designed PPy-based MEAs with a high stretchability (∼100%) and electrode-substrate adhesion (1.9 MPa).[88] Experimental results showed that the PPy microelectrodes exhibited better biocompatibility than the metal counterparts. PEDOT:PSS is one of the most widely investigated conductive polymers for microelectrode applications because of its excellent electrical conductivity,[89] optical transparency,[90,91] biocompatibility and chemical stability,[92,93] and commercial availability. Microelectrodes made of PEDOT:PSS alone could achieve a low normalized 1 kHz impedance at 0.33 $\Omega\cdot cm^2$ and a high optical transparency up to 97% for neural recording.[94] The electrochemical and mechanical properties of conductive polymers can be controlled by doping. For example, transparent PEDOT:PSS films with high stretchability were achieved by mixing PEDOT:PSS with either ionic additives or plasticizers such as Zonyl and Trion.[95−98] The conductivity of a stretchable PEDOT:PSS film blended with conductivity enhancers and ionic additives was >3100 S/cm at 0% strain, >4100 S/cm at 100% strain, and remained >100 S/cm under 600% strain.[95] Donaldson et al. reported inkjet-printed PEDOT:PSS transparent microelectrodes with a ring-shaped design to allow the encapsulated portion of the microelectrodes near the contact site for contributing to signal transduction as well, which improved the impedance and the CSC performance.[99] The 1 Hz impedance reduced from 294 ± 21 to 98 ± 2 kΩ while the CSC enhanced from 6 to 21 mC/cm^2 when the outer diameter of the encapsulated microelectrode increased from 300 to 550 μm, respectively. The microelectrodes exhibited an optical transmittance ∼80% and remained functional after 1000 mechanical bending cycles against a small radius of 2 mm.

2.4. Metallic Nanowires. Metallic nanowires (MNWs) are another attractive material candidate for transparent microelectrodes due to their high conductivity, straightforward synthesis scalability, solution processability, excellent mechanical flexibility/stretchability, and superior optical transparency. Similar to CNTs, the mechanical flexibility/stretchability of MNWs network results from the intersliding behavior of the nanowires in the network. As a result, the electrical performance of a MNW network could easily withstand bending and stretching tests. For instance, Miller et al. demonstrated that the electrical resistance of Ag NWs networks remained stable up to 76% tensile strain and 250 cycles of stretching at 15% strain.[100] Individual MNW has very good electrical conductivity from the bulk metal. The electrical performance decreases when the diameters of individual MNWs approach the mean free path of electrons in the bulk metal (∼40 nm for silver (Ag) or gold

https://doi.org/10.1021/acsabm.3c00131
ACS Appl. Bio Mater. 2023, 6, 1701−1719

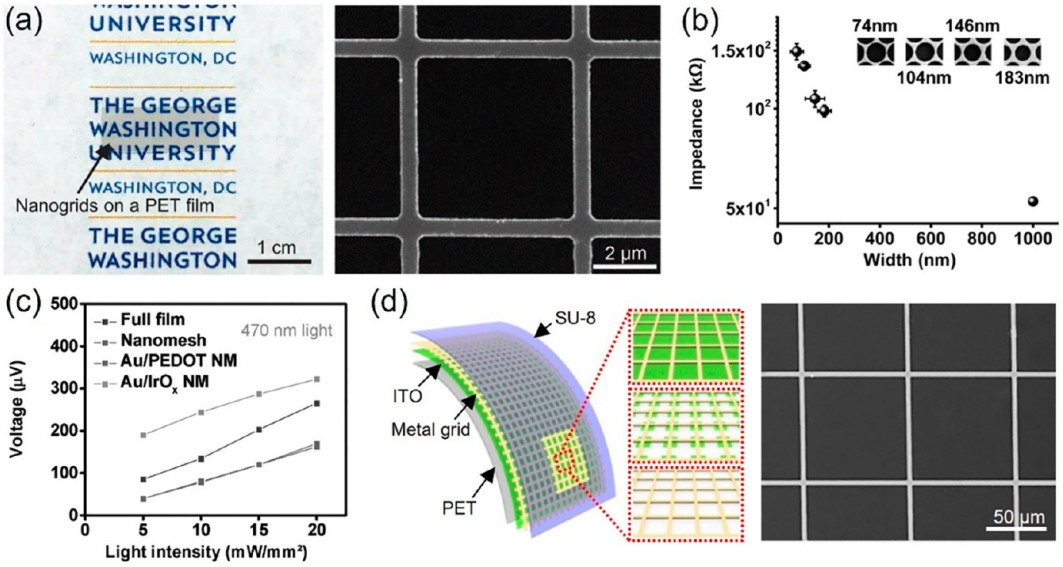

Figure 3. Patterned metal structure-based transparent microelectrode materials. (a) (Left) Optical image of a Au nanogrid/PET film. (Right) SEM image of the Au nanogrid. Reproduced from ref 109. Copyright 2020, Wiley. (b) Impedance versus nanomesh width (thickness 40 nm, microelectrode size 80 μm × 80 μm). Reproduced from ref 30. Copyright 2017, American Chemical Society. (c) Photoelectric artifacts of Au full film, Au nanomesh, Au/PEDOT:PSS nanomesh, Au/IrO_x nanomesh microelectrodes versus 470 nm blue light intensity. Reproduced from ref 115. Copyright 2017, Wiley. (d) (Left) Illustration of hybrid transparent microelectrodes based on metal grid/ITO stuctures. (Right) SEM image of an Au grid/ITO film. Reproduced from ref 116. Copyright 2020, Wiley.

(Au)). Bid et al. reported that the electrical resistivity of Ag NWs increased by 25% when the diameter decreased from 100 to 30 nm.[101] Larger diameters are associated with higher surface roughnesses, which are desired for microelectrodes to increase the effective electrode/electrolyte interfacial area. Meanwhile, a small diameter is beneficial for increasing the optical transmittance by decreasing the proportion of photons scattered and absorbed by the MNWs. The interconnections between different nanowires in the network and the network density play key roles in determining the resulting electrical and optical properties of the MNW microelectrodes. The interconnections can be improved by thermal annealing,[102,103] mechanical pressing,[104] chemical treatments,[105] or laser sintering.[106] Similar to CNT networks, a MNW network that is too sparse does not provide enough efficient pathways for electrons to reach a high conductivity or sufficient surface areas to achieve a superior electrochemical impedance, while one that is too dense becomes too opaque with dramatic losses in the transparency. Chen et al. reported Ag NW-based transparent microelectrodes with a high optical transparency of >90% and a low normalized 1 kHz electrochemical impedance of 3.4−15 Ω·cm^2 by varying Ag NWs network densities.[28] To overcome potential chemical stability and biocompatibility concerns of Ag NWs for chronic or implantable applications, noble metals such as Au have been coated on Ag NWs to form core−shell structure Au-coated Ag NWs (Au−Ag NWs) by several groups.[107,108] For example, Choi et al. demonstrated that the Au sheath significantly reduced the accumulation of Ag ions in various organs and lowered the inflammatory responses and fibrotic reaction in the Au−Ag NWs compared to Ag NWs after being implanted on rat hearts for 3 weeks.[107]

2.5. Patterned Metal Structures. In addition to the intrinsically transparent microelectrode materials discussed above, advanced structure designs that pattern metal materials into porous structures such as grids or meshes represent another important research trend to yield high optical transparency while minimizing the loss of electrical performance of nontransparent metal conductors. Common fabrication processes for the porous structures include lithography,[30,109] printing,[110,111] laser sintering,[112] etc. The geometry and grid/mesh properties (e.g., grid width, thickness, pitch, etc.) of the porous metal structures can be adjusted to achieve balanced electrical and optical properties. For example, for a square metal grid structure, the optical transparency (T) and R_{sh} are determined by the following equations:[113,114]

$$T = 1 - f_F \tag{1}$$

$$R_{sh} = \xi \frac{\rho}{f_F} \frac{1}{h} \tag{2}$$

Here, f_F is the geometrical filling factor defined by (pitch-width)^2/pitch^2, ξ is a correction factor determined by the materials and grid properties, ρ and h are the resistivity and thickness of the grid, respectively. Obaid et al. reported that the optical transmittance of an Au nanogrid (width 500 nm and thickness 40 nm) microelectrode improved from 73.2% to 88.7% while the 1 kHz impedance increased from 59.3 ± 3.54 to 477 ± 19.0 kΩ when the nanogrid pitch increased from 5.5 to 15.5 μm.[109] Figure 3a presents a flexible nanogrid transparent film and SEM image of the Au nanogrids. Seo et al. developed an ultrathin flexible Au nanomesh microelectrode (thickness 15 nm) with a normalized 1 kHz impedance at 8.14 Ω·cm^2 and >65% average transmittance from 300 to 1100 nm using nanosphere lithography methods (Figure 3b).[30] Cell viability and adhesion on the Au nanomesh were tested by incubating mouse embryonic fibroblast cells on the microelectrodes. The nanomesh substrates did not introduce any adverse effects on the cell viability after 7 days.

The electrochemical performance of metal grid/mesh microelectrodes could be improved by low impedance surface coating or designing hybrid composite materials without sacrificing optical transparency. For example, Qiang et al. demonstrated

https://doi.org/10.1021/acsabm.3c00131
ACS Appl. Bio Mater. 2023, 6, 1701−1719

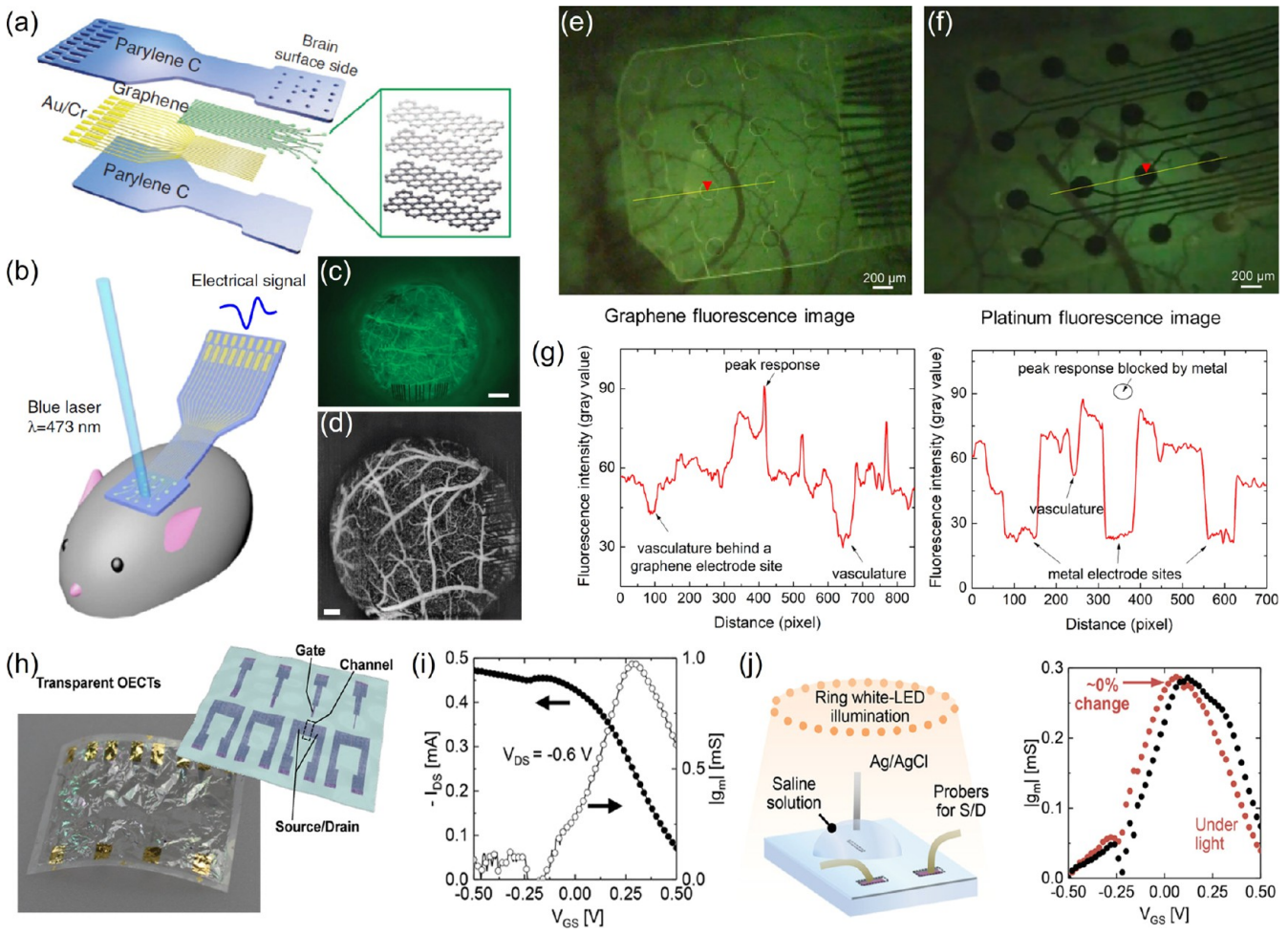

Figure 4. Nonpenetrating flexible transparent recording and stimulation neural MEAs. Schematic illustrations of the CLEAR device (a) and the opto-experimental setup (b). (c) Fluorescence image of the CLEAR device on the cortex of a mouse. Scale bar, 500 μm. (d) OCT angiogram showing the cortical vasculature through the CLEAR device. Scale bar, 200 μm. Reproduced from ref 25. Copyright 2014, Springer Nature. Fluorescence images of a GCaMP6 mouse cortex with a transparent graphene ECoG MEA (e) and an opaque Pt MEA (f). (g) Fluorescence intensity over graphene microelectrodes (left) (data from yellow dotted line in (e)) and Pt microelectrodes (right) (data from yellow dotted line in (f)), respectively. Reproduced from ref 44. Copyright 2018, American Chemical Society. (h) A transparent and ultrathin OECT array. (i) Electrical characteristics of the transparent OECT. (j) (Left) Schematic illustration of OECT measurements under illumination from a white LED. (Right) Transconductance characteristics with and without the white LED illumination. Reproduced from ref 126. Copyright 2023, Wiley.

high-performance bilayer nanomesh microelectrodes by electroplating PEDOT:PSS or IrO_x on the Au nanomesh structures to form faradaic interfacial layers.[115] The electrochemical and optical performances were adjusted by tweaking the thickness of the coating materials. With this strategy, the Au/PEDOT:PSS bilayer nanomesh microelectrodes achieved a 550 nm transmittance of >70% and a 1 kHz impedance at ~10 kΩ, which was 20 times lower than that of the graphene microelectrodes at the same size. In addition, the bilayer nanomesh microelectrodes exhibited much less photoelectric artifacts (40 μV) compared to Au full film microelectrodes (100 μV) under 5 mW/mm^2 blue light irradiance (Figure 3c). Chen et al. developed metal grid/ITO hybrid microelectrodes where the intrinsically transparent patterned ITO islands or uniform ITO films occupied the vacant space of the metal grids to significantly increase the effective interfacial areas between the electrode and electrolyte without changing the geometrical microelectrode areas (Figure 3d).[116] The resulting metal grid/ITO island hybrid microelectrode showed a high optical transparency at 81% from 400 to 800 nm with a low R_{sh} at 14.1 Ω/sq and a normalized 1 kHz impedance at 18.4 Ω·cm^2 while the pure metal grid showed a R_{sh} at 26.8 Ω/sq and a normalized 1 kHz impedance at 212.1 Ω·cm^2. Importantly, the hybrid microelectrodes possessed the mechanical flexibility of the soft metal grid structures instead of the brittle ITO where the R_{sh} of the hybrid structures remained stable after 5000 bending cycles against a small radius of 5 mm. The mechanical softness and durability of patterned metal structures have been further evaluated by multiple groups. For example, Guo et al. reported that grain lithography-prepared Au nanomesh exhibited excellent mechanical robustness with no signs of fatigue or changes in electrical resistance up to 40% tensile strain.[117] Jin et al. reported that a hybrid Ag grid/PEDOT:PSS structure could exhibit superior mechanical stability up to 10,000 bending cycles at a small bending radius of 1 mm.[118]

3. SOFT TRANSPARENT MEAS FOR NEURAL AND CARDIAC APPLICATIONS

Recent developments of transparent MEA systems have mainly focused on applications to the brain and heart because they are among the most vital components of the human body and make up many human diseases.[14,119] In this section, we focus on

https://doi.org/10.1021/acsabm.3c00131
ACS Appl. Bio Mater. 2023, 6, 1701−1719

flexible or stretchable transparent MEAs and their applications as neural and cardiac interfaces in both nonpenetrating and penetrating structure designs based on the transparent conductor materials and structures discussed in Section 2. Specifically, based on the reported design approaches, we discuss (i) flexible nonpenetrating transparent MEAs for neural interfacing with reduced mechanical mismatch, (ii) stretchable nonpenetrating neural transparent MEAs that can accommodate the strain/deformation of brain tissues, (iii) soft penetrating transparent MEAs to probe deeper brain regions, and (iv) soft conformal transparent MEAs for cardiac investigations.

3.1. Flexible Nonpenetrating Transparent MEAs Based Neural Interfaces. Neural MEAs may be classified into nonpenetrating and penetrating geometries. Nonpenetrating electrocorticography (ECoG) MEAs could electrically record neural activity in a less invasive way than penetrating MEAs while having better signal quality than electroencephalography (EEG) MEAs.[14] The mechanical softness feature of nonpenetrating MEAs would allow them to maintain conformal contact with the brain surface for effective interfacing. Early flexible transparent MEAs were demonstrated for ECoG recordings from the cortical surface with simultaneous optical imaging or optogenetic modulation using single- or few-layer graphene sheet-based microelectrodes.[25,26] The graphene films were grown by chemical vapor deposition (CVD) on copper foils, then transferred to flexible polymer substrates via wet transfer techniques and patterned by photolithography and reactive ion etching (RIE). An inherent trade-off between optical transparency and electrical conductivity/impedance exists for graphene MEAs, where more graphene layers improve the electrical conductivity/impedance but decrease the optical transparency. In one example, the 16 channel graphene-based, carbon-layered electrode array (CLEAR) device was patterned on a transparent parylene C substrate (Figure 4a).[25] The microelectrodes included four layers of graphene to achieve a lower R_{sh} (76 Ω/sq compared to 152 Ω/sq in single layer graphene) and a higher fabrication yield. The resulting microelectrodes (200 μm in diameter) exhibited >90% optical transparency from the ultraviolet to infrared (IR) region of the spectrum and a 1 kHz impedance of ∼240 kΩ. The mechanical flexibilities of the devices allowed them to conform to brain surface areas (Figure 4b) for electrical recording of optogenetically evoked neural signals, fluorescence imaging (Figure 4c), and imaging of the cortical vasculature through optical coherence tomography (OCT) (Figure 4d). In a separate but related work, doped graphene MEAs were fabricated on thin polyimide substrates (thickness 12.5 μm) for simultaneous electrical recording and calcium imaging.[26] The chemical doping was achieved by exposing the graphene surface to nitric acid, resulting in the adsorption of NO_3^- groups. Due to the relative high R_{sh} of the graphene layers, Au interconnects and bonding pads were used. A significant improvement in SNR and reduction in electrical interference noise compared to solid Au electrodes were realized. The 16 channel graphene MEAs showed ∼80% transparency and a 1 kHz impedance of 541 kΩ with an individual microelectrode size of 50 μm × 50 μm. The electrical signals from the hippocampal tissue recorded by graphene MEAs aligned well with the colocalized calcium transients from confocal microscopy setups. The combination of the two recording modalities unraveled both the spatial and temporal characteristics of the high-frequency oscillations and synaptic potentials. In another work by Thunemann et al., it was demonstrated that crack- and residue-free flexible and transparent graphene MEAs could be realized by optimizing (1) the graphene transfer and (2) photoresist and organic residue removal from graphene surfaces during the fabrication process.[120] More recently, transparent graphene ECoG MEA has been combined with calcium imaging to unravel the state transitions in the temporal and spatial progression of seizures, with potentials to enable targeted therapeutic interventions in the future.[121]

In addition to ECoG recording, Park et al. later developed another transparent CLEAR device for simultaneous electrical stimulation of the cortex with *in vivo* optical monitoring.[44] The charge density of the capacitive four-layer graphene microelectrodes (17,671 μm^2) could reach 116.07−174.10 $\mu C/cm^2$. The electrical stimulation evoked calcium fluorescence was clearly visible in the CLEAR device while obstructed in an opaque Pt MEA (Figure 4e−g).

More recently, PEDOT:PSS-based soft and transparent ECoG MEAs are developed from solution processing-based fabrication techniques, which avoid the additional transferring process in the aforementioned graphene MEAs.[27] For example, Cho et al. reported a transparent MEA composed of a single layer of ethylene glycol (EG)-treated PEDOT:PSS as both the interconnects and microelectrodes on a transparent PET substrate. The fabrication adopted a facile ultrasound lift-off process with spin-coated PEDOT:PSS dispersion. EG treatment dramatically improved the conductivity and electrochemical performance of the PEDOT:PSS microelectrodes without sacrificing optical transparency (85%). The 1 kHz impedance value of the 16 PEDOT:PSS-EG microelectrodes (300 μm × 300 μm) in the MEA ranged from 50 to 70 kΩ. The transparent PEDOT:PSS-EG MEA allowed blue light from a laser to accurately transmit to the right cerebral cortex areas expressing blue light-activated opsin ChR2 underneath the MEA and recorded the optically evoked changes in neural activity. In comparison, an opaque Au MEA exhibited much less light-evoked neural activity due to its low optical transmittance. The biocompatibility of the PEDOT:PSS-EG MEA was assessed with cell proliferation experiments using primary cortical neurons and PC12 cells for 6−7 days. No statistically significant differences in cell viability were observed between the MEA and a glass control substrate, suggesting the excellent biocompatibility of the PEDOT:PSS-EG MEA. In another example, Donaldson et al. demonstrated transparent PEDOT:PSS MEA for simultaneous electrical and optical recording of cortical dynamics from multiple brain regions.[122] The patterning and fabrication of the MEA relied on inkjet printing of Ag interconnects and bond pads and 200 nm thick PEDOT:PSS microelectrodes (50 μm in diameter) on laser patterned PET substrates, followed by parylene C encapsulation. The 10 microelectrodes in the MEA spread over a window with a large field of view of ∼45 mm^2 for simultaneous optical imaging. The fully assembled implant only weighed ∼1.4 g, which is suitable for chronic applications in small animals. The performance of the microelectrodes remained stable after implantation *in vivo* over 100 days.

To achieve MEAs with high spatial resolution, microelectrodes with sizes comparable to those of single neurons (∼10−20 μm) are preferred.[14] In this context, the most challenging technical issue was how to maintain an excellent impedance performance for high-fidelity recording at such small sizes. To resolve this challenge, Qiang et al. developed flexible and transparent 32 channel MEAs with Au/PEDOT:PSS bilayer nanomesh structures on a parylene C substrate using a

https://doi.org/10.1021/acsabm.3c00131
ACS Appl. Bio Mater. 2023, 6, 1701−1719

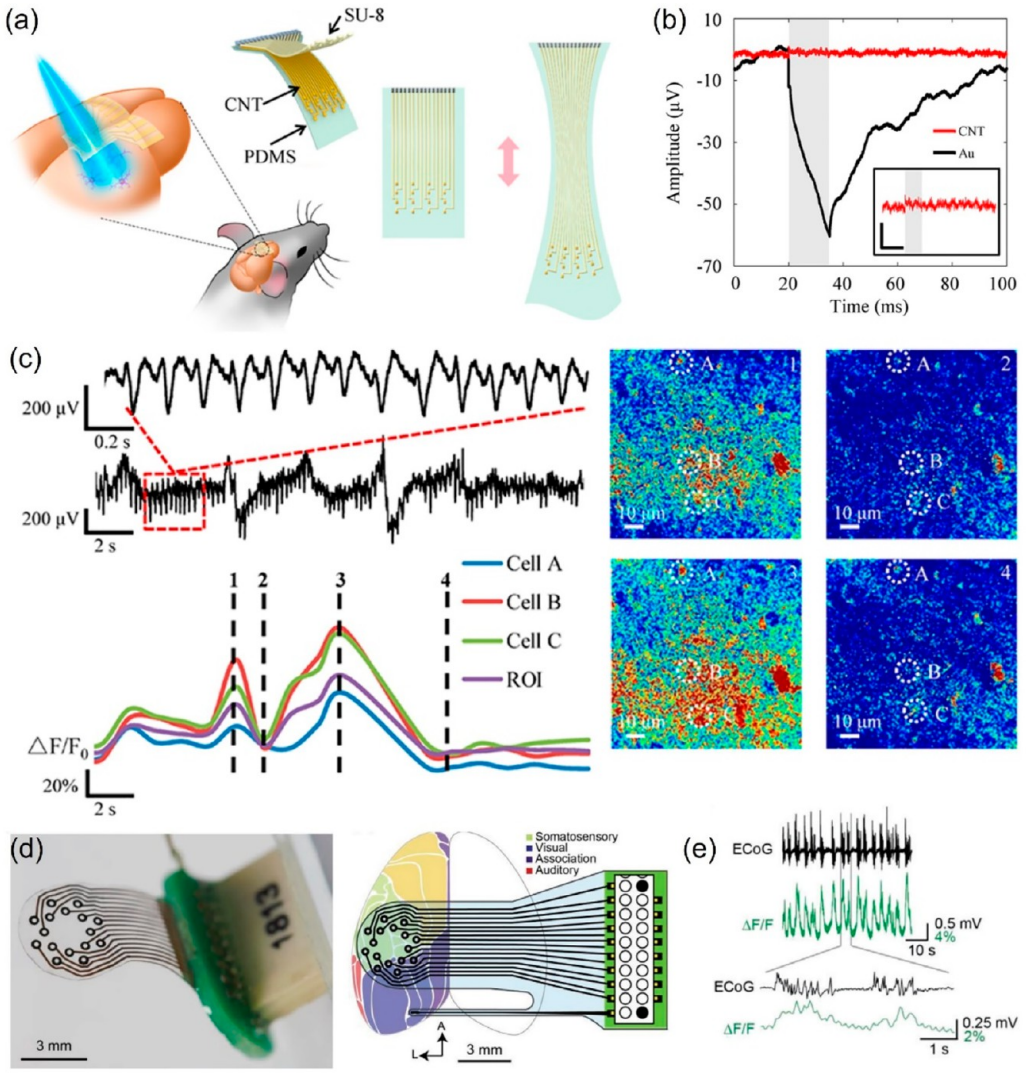

Figure 5. Nonpenetrating stretchable transparent neural MEAs. (a) Schematic illustration of a CNT transparent MEA. (b) Minimized photoelectric artifacts from a CNT microelectrode compared to a Au microelectrode. (c) Simultaneous CNT microelectrode recorded electrical signals (top left) and optical calcium transients under the CNT microelectrode (bottom left) during seizure-like events. (Right) Two-photon images for the four dashed timelines on optical calcium transients. Reproduced from ref 128. Copyright 2018, American Chemical Society. (d) (Left) Photograph of a 16 channel Au NWs ECoG array. (Right) Schematic illustration of the MEA covering multiple regions of interest in the cortex of a mouse. (e) Representative correlated ECoG signals from the MEA and two-photon calcium fluorescence signals. Reproduced from ref 129. Copyright 2020, Wiley.

nanosphere lithography method.[31] The PEDOT:PSS layer (thickness 85 nm) was electroplated on the Au nanomesh surface (mesh thickness 25 nm, mesh width 70 nm, and mesh pitch 1 μm). The resulting MEAs exhibited 70% optical transmittance in the visible range. The 1 kHz impedance (130 kΩ) of a single microelectrode (20 μm diameter) was on par with that of the nontransparent Michigan arrays and >20 times lower than graphene or ITO microelectrodes with the same size and optical transparency. The bilayer nanomesh MEAs enabled simultaneous recording of the electrical activity of awake mice with additional two-photon calcium imaging of a single neuron in the visual cortex. The action potentials were classified into six frequency bands (α, β, γ, high γ, ultrahigh γ, and multiunit). The electrical signals below the α band (8−12 Hz) contained the same temporal information as calcium imaging while the results in higher frequency bands contained information on much faster events beyond those that could be monitored by calcium imaging, highlighting the benefits of multimodal electrical and optical recordings for neuroscience research.

Compared to passive MEAs that require one wire per microelectrode, active MEAs can potentially record signals with a higher spatial resolution and allow integration of a larger number of microelectrodes in the same geometrical area. This is because each row and column of microelectrodes in the active MEAs could be connected with only one wire and controlled by multiplexing transistors to significantly reduce the number of interconnects.[123,124] To leverage such advantages, flexible and transparent organic electrochemical transistors (OECTs) using conductive polymers as channels are recently developed. For example, Lee et al. designed a 3 μm thick 3 × 5 flexible active MEA consisting of transparent OECTs with PEDOT:PSS as the active layer and Au grid wirings as the source/drain and interconnects on the surface of a rat brain.[125] The Au grid was fabricated by a photolithography and lift-off process. PEDOT:PSS was prepared by spin coating and patterned by

https://doi.org/10.1021/acsabm.3c00131
ACS Appl. Bio Mater. 2023, 6, 1701−1719

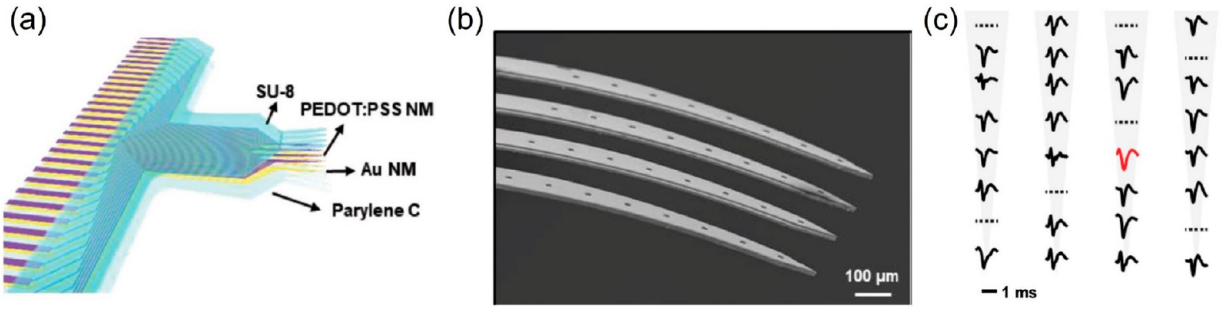

Figure 6. Penetrating transparent neural MEAs. (a) Schematic of a 32 channel transparent Au/PEDOT:PSS bilayer nanomesh penetrating MEA. (b) SEM image of four shanks of the MEA. (c) Average spiking activity recorded by each channel in the MEA from the visual cortex of an anesthetized mouse. Dashed dots indicated no spike detected at the channel. Reproduced from ref 131. Copyright 2019, Wiley.

dry etching. The optimized Au grid wirings had a grid width of 3 μm and a pitch of 18 μm, with an optical transmittance of 69% and a R_{sh} of 3 Ω/sq. This device demonstrated a 1 kHz impedance of 10 kΩ with a microelectrode size of 1400 μm^2. The optogenetically evoked ECoG signals by a 473 nm laser beam from the transparent OECTs exhibited twice the amplitude (700 μV) with minimized reflections of laser stimulation compared to reference nontransparent OECTs. More recently, Takemoto et al. developed another flexible and transparent OECT array with Ag NWs electrodes and a PEDOT:PSS channel (Figure 4h).[126] The Ag NWs source/drain electrodes and 180 nm thick PEDOT:PSS active layer were patterned on a 1 μm thick parylene C substrate via selective wetting deposition using rod coating with a high resolution down to 20 μm. The encapsulation parylene was bonded via the thermal lamination. The electrodes exhibited a high optical transmittance of >90% in the visible region and a low R_{sh} of 25 Ω/sq. A high transconductance of ∼1 mS was obtained in low-voltage operations (<0.6 V, Figure 4i), comparable to that of the typical OECTs using Au source/drain electrodes. Figure 4j shows that the gate voltage at peak transconductance was insensitive to white light irradiance (2.3 mW/cm^2).

3.2. Stretchable Nonpenetrating Transparent MEA-Based Neural Interfaces. A moderate to high stretchability of the MEAs is desired for applications in mechanically active environments because they can form an intimate contact with soft tissues (e.g., curvilinear brain or heart surfaces) and withstand the repetitive strains induced by vital body functions such as breathing and heart contraction (e.g., strain levels ∼10% and 20% in the brain and heart, respectively).[88,127] Zhang et al. reported stretchable and transparent MEAs integrating CNT microelectrodes, PDMS elastomer substrate, and SU-8 encapsulation (Figure 5a).[128] CNT films were grown by CVD and patterned on a copper foil sacrificial substrate with the SU-8 encapsulation layer by a RIE process. A PDMS layer was spin coated on the CNT/SU-8 pattern side, followed by selective wet etching to remove the copper foil sacrificial substrate and release the MEAs. PDMS is ultrasoft, biocompatible, and transparent and has a low sensitivity to the media's osmolarity or pH. The elastic properties of PDMS can be controlled by using different PDMS materials and varying the ratio between base and cross-linker components. As a result, PDMS has been widely used as a stretchable and transparent substrate candidate for bioelectronics. The MEAs exhibited an optical transmittance of >85% in the visible and IR range with only a 26% increase in impedance under a tensile strain of 20% due to the stretchability of the percolation CNT network. In comparison, the impedance of graphene microelectrodes increased >10 times upon only 3% of tensile strain. The photoelectric artifacts were undetectable for the CNT microelectrodes when exposed to 2.4 mW/mm^2 blue light illumination while the artifacts from opaque Au microelectrodes were ∼60 μV (Figure 5b). Figure 5c presents concurrent ECoG signals and two-photon calcium imaging results from GCaMP expressing cortical neurons under the CNT MEAs during a seizure-like ictal event. The calcium imaging captures the contributions of individual neurons in the complex network while the CNT electrical recording enables detection of high frequency population discharges at a high temporal resolution without perturbing either sensing mode. In another example, a 16 channel stretchable and transparent ECoG MEA was fabricated from Au NWs on PDMS (Figure 5d).[129] The fabrication process contains three main steps, including photolithographic patterning of filter membranes as masks, filtration of Au NWs or Pt particles through these masks, and embedding the conductive components into patterns in PDMS. The MEAs showed 90% optical transparency and a 1 kHz impedance of 1 kΩ with a microelectrode size of 94,200 μm^2. The MEAs were chronically stable *in vivo* for weeks and suitable for simultaneous two-photon calcium imaging and ECoG recording in awake and anesthetized animals. The calcium signals exhibited a correlation in positive and negative peaks with the ECoG results where the ECoG signals exhibited faster temporal dynamics (Figure 5e), and fluorescence imaging provided higher spatial resolution across the full field of view.

3.3. Soft Penetrating Transparent MEA-Based Neural Interfaces. ECoG or EEG recording and stimulation MEAs are not sufficient to probe neural activity in deeper brain regions. Soft transparent penetrating MEAs that can probe different depths of the brain would complement those aforementioned nonpenetrating transparent MEAs and yield additional information. Lee et al. produced an intracortical "micro-optoelectrode array" from the optically transparent wide bandgap semiconductor zinc oxide (ZnO).[130] The device was fabricated from a ZnO bulk single crystal and consisted of a 4 × 4 array of electrically isolated shanks (each 1.5 mm long, 400 μm pitch) in a form factor similar to the Utah array. ZnO served as both the electrical recording channel and optical waveguide (∼200 kΩ impedance, >70% transparency, refractive index ∼2.0) with a parylene C cladding layer (refractive index ∼1.6) so optical power could be transmitted to the exact position of the electrical recording sites. The resulting device allowed combination of different optical and electrical functions (electrical recording and stimulation with optical stimulation and recording) at the tip of each individual channel at an ∼1.5

https://doi.org/10.1021/acsabm.3c00131
ACS Appl. Bio Mater. 2023, 6, 1701−1719

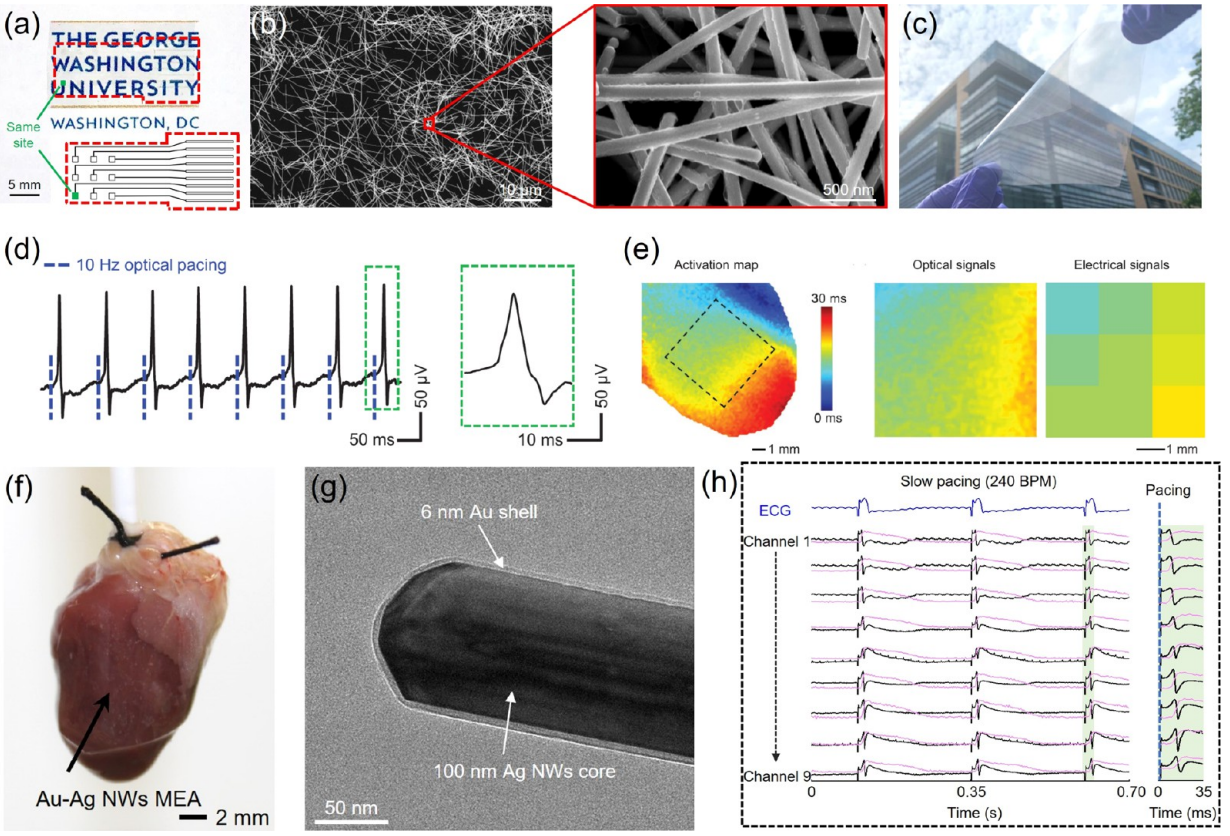

Figure 7. Soft transparent cardiac MEAs. (a) Optical image of a 3 × 3 flexible and transparent Ag NWs MEA and interconnects. (Inset) Schematic of the MEA design. (b) SEM images of the Ag NWs network in the MEA. (c) Optical image of a 10 cm × 10 cm large area Ag NWs film. (d) EG recording results from the transparent Ag NWs microelectrodes during colocalized 10 Hz optogenetic pacing of a mouse heart. (e) (Left) Optical activation map recorded from the left ventricle region of a rat heart. The Ag NWs MEA area was highlighted by the black dashed square. (Right) Simultaneous electrical and optical activation maps obtained from the area under the Ag NWs MEA. Reproduced from ref 28. Copyright 2021, Wiley. (f) Optical image of a stretchable and transparent Au−Ag NWs MEA conformally laminated on the left ventricle epicardium of a rat heart. (g) Transmission electron microscopy image of a core−shell structure Au−Ag nanowire. (h) Representative ECG signals (blue), colocalized and time aligned 9 channel EG signals (black) and optical transmembrane potential mapping signals (magenta) captured simultaneously during electrical pacing conditions. Reproduced from ref 108. Copyright 2023, Wiley.

mm depth into the brain. More recently, progress has been made to develop penetrating MEAs with improved mechanical softness. For example, Seo et al. demonstrated a flexible and transparent penetrating 32 channel MEA consisting of Au/PEDOT:PSS bilayer nanomesh microelectrodes on a parylene C substrate (Figure 6a).[131] The microelectrodes exhibited a 1 kHz impedance of 149 kΩ with sizes of 15 μm × 15 μm to measure single-unit action potentials in the brain and a 67% optical transparency at 550 nm. The MEA showed great mechanical robustness with negiligible changes in impedance after 1000 bending cycles against a 4 mm small bending radius. The largest cross-sectional footprint of each shank is 20 μm × 90 μm, which is beneficial to reduce the tissue damage during implantation. Due to the extreme softness of the parylene C shanks (Figure 6b), polyethylene glycol was used as a biocompatible stiffener to temporarily harden the MEAs for better insertion into the intracortical areas of the brain. Figure 6c presents the recorded single-unit neural activity across multiple layers of the mouse visual cortex by the penetrating MEA.

3.4. Soft Conformal Transparent MEAs for Cardiac Interfaces. Cardiovascular diseases are a leading cause of morbidity and mortality worldwide.[132,133] Due to their complex underlying pathophysiology and immediate threat to life, they are also among the most challenging human diseases to diagnose and treat. In recent years, soft transparent MEAs have become attractive tools to interface with beating hearts for crosstalk-free integration of electrical recording/stimulation with optogenetic modulation or optical mapping, which allows for a comprehensive investigation of heart functions in health and disease. Chen et al. reported flexible and transparent 9 channel Ag NWs MEAs for cardiac applications in 2021 (Figure 7a).[28] The Ag NWs structures were fabricated on transparent PET substrates using fully solution-based photolithography steps where the transparent Ag NWs networks (Figure 7b) served as both the transparent microelectrodes and interconnects. This design not only simplified the device fabrication process but also enabled optical probing of the whole device area. The solution processing-based fabrication techniques had a high patterning resolution of ∼15 μm and could enable high-channel-count transparent MEAs for large-scale cardiac mapping (Figure 7c). The MEAs and interconnects exhibited a high optical transparency of >90% at 550 nm, a normalized 1 kHz impedance down to 3.4 Ω·cm^2, a low R_{sh} of 4.1 Ω/sq, and a superior mechanical flexibility with no changes in electrical performance up to 100,000 bending cycles at a 5 mm radius. Studies on Langendorff-perfused mouse and rat hearts demonstrated that the Ag NWs MEAs enabled high-fidelity real-time monitoring of heart rhythm during colocalized optogenetic pacing (Figure 7d) and optical mapping (Figure 7e). The optical mapping signals represented the average results over ∼0.5 to 1 mm of depth

https://doi.org/10.1021/acsabm.3c00131
ACS Appl. Bio Mater. 2023, 6, 1701−1719

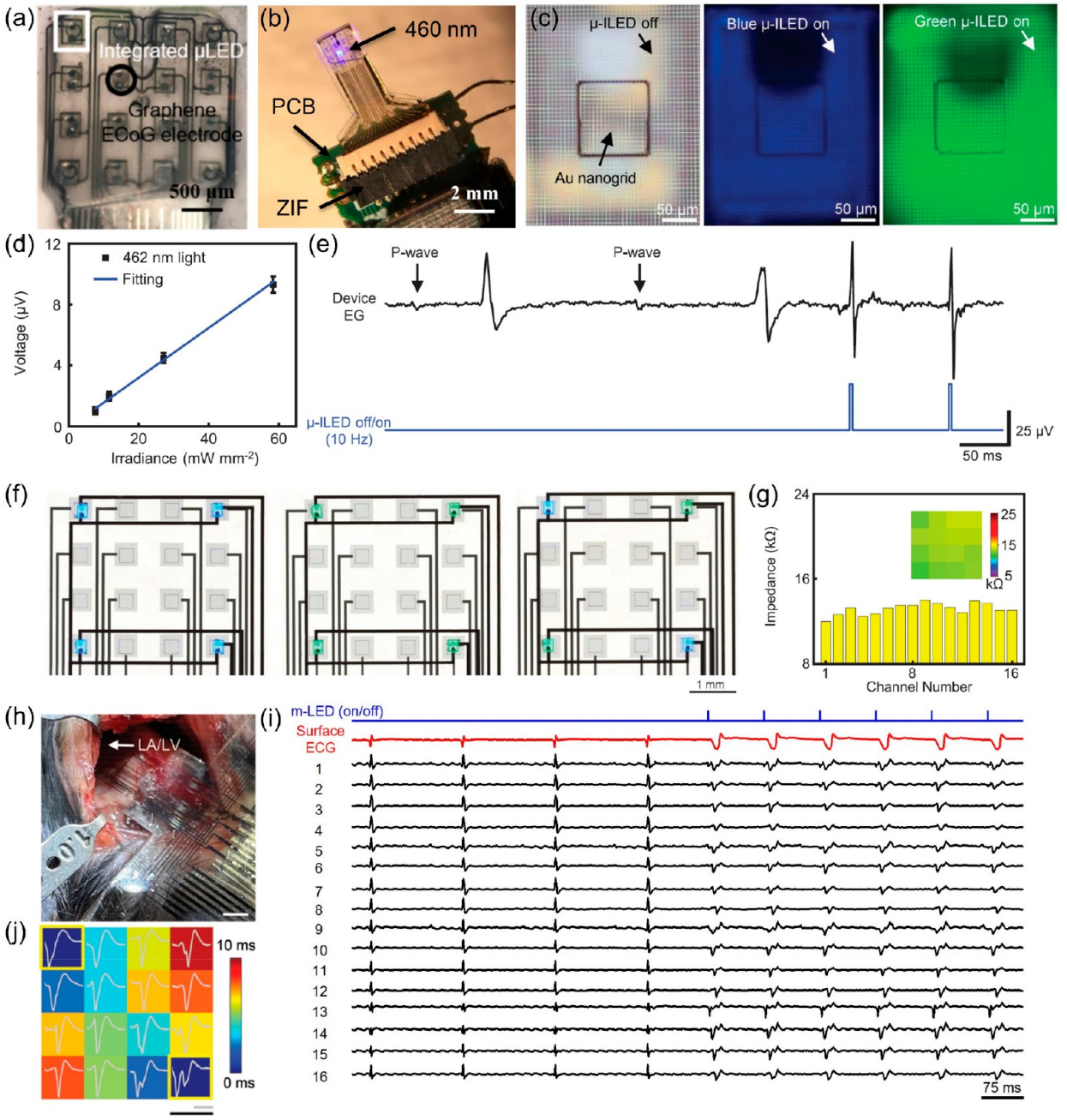

Figure 8. Soft transparent microelectrode-based hybrid opto-electric devices for simultaneous electrical recording and optogenetics. (a) Optical image of a blue μ-LED integrated graphene MEA device. (b) Photography of a fully assembled device with the connector and 1 μ-LED emitting blue light. Reproduced from ref 138. Copyright 2021, American Chemical Society. (c) Optical images of multifunctional opto-electric devices integrating Au nanogrid microelectrodes with blue and green μ-LEDs. (d) Photoelectric artifacts of the Au nanogrid microelectrodes versus different irradiances from the blue μ-LEDs in the opto-electric devices. (e) EG recording signals from an opto-electric device showing the detection and termination of AV block via optogenetic pacing with the blue μ-LED in the same device. Reproduced from ref 109. Copyright 2020, Wiley. (f) Optical images of multilayered opto-electric array devices with 4 μ-LEDs and 16 Au grid microelectrodes. (g) Impedance histogram of the 16 Au grid transparent microelectrodes in the opto-electric array devices. (h) Optical image of an opto-electric array device contacting the beating mouse heart *in vivo*. (i) *In vivo* 16 channel EG mapping results during sinus rhythm and optogenetic pacing using the μ-LED in the bottom left corner of the opto-electric array devices. (j) Electrical activation map during multisite optogenetic pacing (pacing sites highlighted by the yellow box). Gray scale bar, 15 ms. Black scale bar, 1 mm. Reproduced from ref 139. Copyright 2022, Wiley.

below the epicardial surface while the electrogram (EG) signals recorded by the Ag NWs MEA were directly from the tissue surface. To form a conformal contact with the mechanically active beating hearts (up to 20% strain), the same group later reported a stretchable version (stretchability of 40%) of the transparent Ag NWs MEA with PDMS encapsulation and substrate layers.[134] The EG signals recorded by the Ag NWs microelectrodes from the epicardial surface of mouse hearts during concurrent optogenetic pacing before and after stretching showed similar morphologies, suggesting their mechanical robustness. More recently, 9 channel highly transparent and stretchable core−shell structure Au−Ag NWs

https://doi.org/10.1021/acsabm.3c00131
ACS Appl. Bio Mater. 2023, 6, 1701−1719

MEAs were developed (Figure 7f).[108] Compared to bare Ag NWs MEAs, electroplating an ultrathin (6 nm) Au shell (Figure 7g) significantly improved the chemical stability, biocompatibility, and electrochemical performance of the Au−Ag NWs MEAs with minimal loss of optical transparency. The resulting Au−Ag NWs MEAs exhibited an optical transparency of ∼80% in the visible region, a low normalized 1 kHz impedance of 1.2 Ω·cm^2, a stable electrochemical performance after exposure to oxygen plasma for 5 min, and cyclic mechanical stretching for 600 cycles at 20% strain. The excellent mechanical stretchability resulted from the use of a PDMS elastomer substrate and photolithographic patterned serpentine-shaped Ag NWs interconnect structure designs, confirmed by finite element analysis. The serpentine structure on elastomer substrates is an effective design to achieve stretchable bioelectronic devices.[135] Figure 7h demonstrates the time-aligned EG signals recorded by the Au−Ag NWs MEA and optically mapped action potentials from the tissue below each microelectrode during electrical pacing. The downward deflections in the EG signals align well with the depolarization phase of the action potentials from colocalized optical mapping. In addition, the voltage-calcium activation delay was precisely extracted by the electrical activation times measured using MEA EG signals and the beginning of intracellular calcium transients from optical calcium fluorescence mapping through the MEAs, which further demonstrated the capability of colocalized mapping of cardiac excitation-contraction coupling using the stretchable Au−Ag NWs MEA.

4. SOFT MULTIFUNCTIONAL OPTO-ELECTRIC DEVICES FOR NEURAL AND CARDIAC INTERFACES

The transparent MEAs in Section 3 all rely on external optical fiber or microscope setups for simultaneous optogenetic modulation or optical mapping. Another important emerging engineering approach to combine electrical and optical modalities is to integrate custom-made or commercially available μ-LEDs and μ-PDs with transparent microelectrodes on a chip. In such hybrid devices, the optical channels will be directly underneath the transparent microelectrodes for colocalized electrical and optical operations around the same sites. Here, electrical recording/stimulation directly takes place at the abiotic/biotic interface. Meanwhile, the underneath μ-LEDs and μ-PDs provide optical light delivery to or receive the local fluorescence signals from the tissue after photons penetrate through the transparent microelectrodes. Those devices are advantageous toward (1) fully wireless multimodal investigations in freely behaving test subjects, (2) multimodal implantable applications in deep tissues where it is very difficult to precisely align the external optical components (e.g., optical fibers) with transparent MEAs without spatial mismatch, (3) studies that prefer focused light illumination to small tissue areas, and (4) simultaneous optical operations at different wavelengths, etc. Meanwhile, the development of transparent microelectrode-based hybrid opto-electric devices is much more challenging compared to transparent MEAs alone due to the requirement to integrate additional optical components in the devices and remains largely unexplored. In this section, we highlight several recent examples in soft hybrid opto-electric devices that combine transparent microelectrodes, light sources, and/or photodetectors on a chip.

4.1. Soft Opto-Electric Devices for Electrical Recording and Optogenetics. Initial soft hybrid opto-electric devices relied on manual bonding of separately fabricated transparent MEA films with films of surface-mounted μ-LEDs using glues or adhesives to accommodate the electrical recording and optogenetic modulation modalities. In one example, Kwon et al. designed a 4 × 4 multichannel Opto-μECoG array combining a transparent MEA and a blue μ-LED array.[136] The μECoG array consisted of transparent ITO microelectrodes (100 nm thick), Au interconnects, and a parylene C substrate (10 μm) for electrical recording (1 kHz impedance between 1 and 5 kΩ) without compromising the optical throughput due to a high optical transmittance of 80%. The μ-LED array was fabricated using commercial blue μ-LED chips (220 μm × 270 μm × 50 μm) with an emission maximum of ∼470 nm by a microtransfer printing and reflow soldering process. The separately fabricated μECoG array and blue μ-LED array were then aligned and bonded together using a 50 μm thick SU-8 adhesive layer. Importantly, a <0.3 °C increase in temperature was observed with the μ-LEDs operating at an input voltage of 2.8 V with an output irradiance of ∼10 mW/mm^2 for optogenetic applications, which was well below the thermal threshold (2 °C) for tissue damage.[137] In another work, Park et al. reported flexible blue μ-LED integrated graphene MEAs where arrays of μ-LEDs were vertically stacked on top of transparent graphene microelectrodes so photons emitted from the μ-LEDs could pass through the microelectrodes for synchronous optical stimulation and electrical recording of the same cells (Figure 8a).[138] The μ-LED array and graphene MEA were fabricated separately on transparent polyurethane and PET substrates. Their backsides were attached and bonded at the array region using a polyurethane glue (Figure 8b). The measured photoelectric artifacts from the graphene MEAs were between 100 and 200 μV with the μ-LEDs operating at different intensities, which were comparable to the artifacts of the transparent graphene MEAs when exposed to external laser light sources.[25,44]

Obaid et al. exploited advanced structure design approaches with suitable materials and reported another flexible opto-electric device design by monolithically integrating transparent Au nanogrid microelectrode on μ-LEDs (Figure 8c).[109] For device fabrication, multicolor μ-LEDs were first microtransfer printed and soldered on photolithographically defined interconnects on PET substrates. The nanogrid microelectrodes were then directly patterned ontop of the μ-LEDs via electron-beam lithography (EBL). The parameters of the nanogrid microelectrodes (e.g., grid width and pitch) could be adjusted by EBL, and the optical profiles of the μ-LEDs could be tuned using commercial μ-LEDs with different emission wavelengths. The microelectrodes exhibited an optical transmittance of >70% in the visible region and a low normalized 1 kHz impedance of 5.9 Ω·cm^2. The photoelectric artifacts from the nanogrid microelectrode during the concurrent operations of the underneath blue μ-LEDs were negligible (Figure 8d) due to the combined effects of high optical transparency and bilayer Cr/Au design where the 15 nm Cr layer prevented the majority of photons from reaching to the Au layer. *Ex vivo* testing on Langendorff-perfused mouse hearts (Figure 8e) showed that the hybrid device could record abnormal heart rhythms such as an atrioventricular (AV) block with the nanogrid microelectrode and restore sinus rhythm through optical pacing at programmed conditions with the μ-LED. The device biocompatibility was evaluated with the devices sutured to the dorsal skin and epicardial surface of rat hearts for 4 weeks. Histological analysis suggested the devices were fully biocompatible. In a more recent study, the same group took a major leap forward and developed flexible opto-electric arrays containing 16 transparent Au grid microelectrodes and 4 multimolor blue and green μ-LEDs at the

https://doi.org/10.1021/acsabm.3c00131
ACS Appl. Bio Mater. 2023, 6, 1701−1719

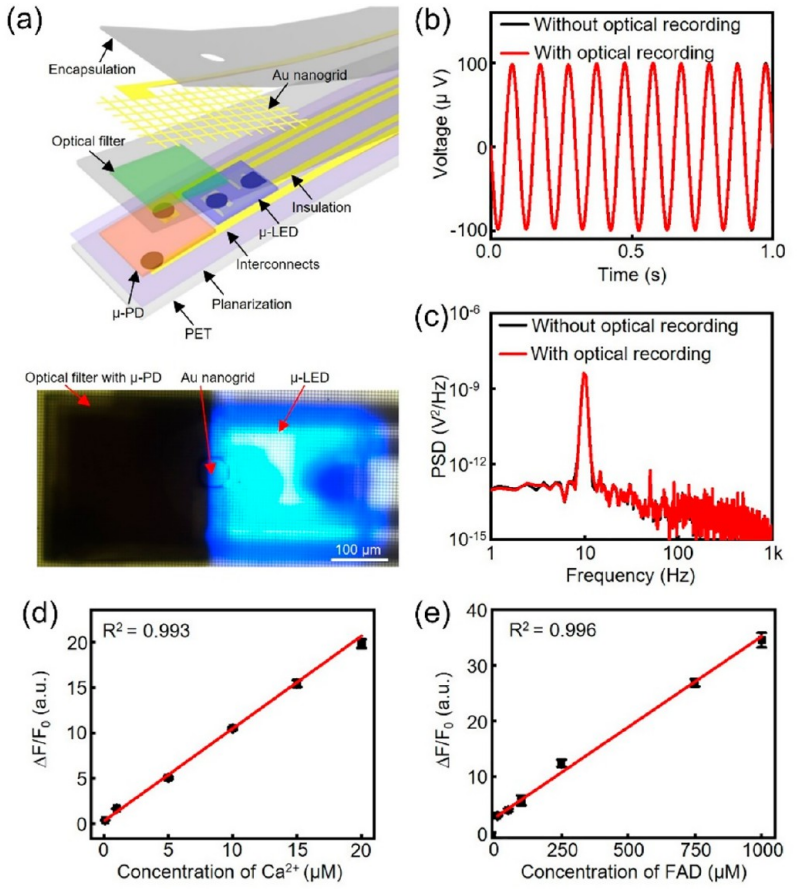

Figure 9. Soft transparent microelectrode-based opto-electric devices for simultaneous electrical and optical recordings. (a) (Top) Schematic of a flexible multimodal opto-electric device integrating a transparent Au nanogrid microelectrode, a blue μ-LED, and a μ-PD with optical filter. (Bottom) Optical image of an opto-electric device. (b) Representative electrical recording output of a 200 μV peak-to-peak sine wave by the transparent Au nanogrid microelectrode in the opto-electric device with and without simultaneous optical calcium fluorescence recording. (c) Representative power spectral density (PSD) graph of the recording results in (b). Fluorescence measurement results from calcium dyes with calcium concentrations ranging from 0.1 to 20 μM (d), and FAD solutions with concentrations ranging from 10 to 1000 μM (e), respectively. Reproduced from ref 140. Copyright 2023, American Chemical Society.

corners (Figure 8f).[139] Each μ-LED had a Au grid microelectrode (grid width 1.5 μm, grid pitch 15 μm) directly on top. The microelectrodes exhibited uniform performance with an average 1 kHz impedance of 13.2 ± 0.56 kΩ (Figure 8g), a CSC of 0.51 ± 0.01 mC/cm^2, and a high optical transparency of >70% from 400 to 800 nm. The array devices allowed colocalized crosstalk-free spatiotemporal cardiac electrical mapping/pacing and optogenetic modulation of animal hearts and human heart slices *ex vivo* and *in vivo* (Figure 8h) to investigate cardiac excitation wave patterns and conduction velocity at both regional and tissue levels on the epicardial surface. Figure 8i shows 16 channel electrical mapping results from the MEA during sinus rhythm and 10 Hz optogenetic pacing from a corner blue μ-LED on a beating heart *in vivo*. Figure 8j presents the activation map from the MEA during multisite optogenetic pacing with 2 μ-LEDs. Multisite pacing reduced the activation time range (9.45 ms) compared to single site pacing (13.4 ms).

4.2. Soft Opto-Electric Devices for Electrical Recording and Optical Recording. Multimodal hybrid opto-electric devices that allow simultaneous monitoring of electrical and optical fluorescence signals at the same site are desirable to leverage the advantages of both methods and help to fully understand the correlation and interaction between the two data types. They are generally much more challenging to build than those hybrid electrical recording and optogenetic modulation tools in Section 4.1 because only μ-LED light sources are required for optogenetics to excite opsins while μ-LEDs, appropriate μ-PDs, and effective on-chip optical filters are needed for fluorescence recording to both excite and selectively record fluorescence from fluorescent reporters. Recently, the Lu group designed and fabricated a flexible and multimodal opto-electric probe that monolithically integrated a blue μ-LED and a μ-PD coated with an effective optical filter beneath a transparent Au nanogrid microelectrode for such applications (Figure 9a).[140] The advanced structure design and fabrication process consists of (1) photolithographic patterning of metal interconnects for the microelectrodes and optoelectronic components, (2) microtransfer printing and reflow soldering to prepare μ-LEDs and μ-PDs, (3) photolithographic patterning of optical filters on μ-PDs, and (4) EBL to generate the Au nanogrids above the μ-LEDs and μ-PDs. The Au nanogrid (grid width 400 nm and pitch 6 μm) featured an optical transmittance of >80% in the visible region and a low normalized 1 kHz impedance of 6.3 Ω·cm^2. Figure 9b and c presents electrically recorded signals of a programmed sine wave during simultaneous optical recording of 1 μM calcium fluorescence signals from the hybrid opto-electric device with no observable crosstalk. By optimizing the conditions of the optical filters, a

https://doi.org/10.1021/acsabm.3c00131
ACS Appl. Bio Mater. 2023, 6, 1701−1719

Table 1. Summary of Characteristics of Transparent Microelectrodes Used in MEAs and Multimodal Opto-Electric Devices

microelectrode materials	optical transmittance	1 kHz impedance (kΩ)	flexible/ stretchable	application	device type	ref.
graphene	~90%	243.5 ± 5.9	flexible	brain (nonpenetrating)	MEA	25
doped graphene	~60−80 (>550 nm)	541	flexible	brain (nonpenetrating)	MEA	26
graphene	>90%	100−600	flexible	brain (nonpenetrating)	MEA	44
PEDOT:PSS	85%	50−70	flexible	brain (nonpenetrating)	MEA	27
PEDOT:PSS	~77%−80%	~16−19	flexible	brain (nonpenetrating)	MEA	122
Au/PEDOT:PSS nanomesh	~70%	130	flexible	brain (nonpenetrating)	MEA	31
PEDOT:PSS OECT	69%	10	flexible	brain (nonpenetrating)	MEA	125
PEDOT:PSS OECT	>90%	10−40 (100 Hz)	flexible	brain (nonpenetrating)	MEA	126
CNT	>85%	200 ± 30	stretchable	brain (nonpenetrating)	MEA	128
Au NWs	>90%	0.998 ± 0.093	stretchable	brain (nonpenetrating)	MEA	129
ZnO	>70%	~200	N/A	brain (penetrating)	MEA	130
Au/PEDOT:PSS nanomesh	67%	149	flexible	brain (penetrating)	MEA	131
Ag NWs	77%−90%	1.2−14.7	flexible	heart	MEA	28
Ag NWs	61%−81%	0.90−1.43	stretchable	heart	MEA	134
Au−Ag NWs	>80%	0.86−9.4	stretchable	heart	MEA	108
ITO	55%−80%	1−20	N/A	brain (nonpenetrating)	multimodal opto-electric	136
graphene	~85%	161	flexible	N/A	multimodal opto-electric	138
Au nanogrid	>70%	59.3−477	flexible	heart	multimodal opto-electric	109
Au microgrid	>70%	6.5−18.5	flexible	heart	multimodal opto-electric	139
Au nanogrid	>80%	157−571	flexible	N/A	multimodal opto-electric	140

high wavelength selectivity >1300 and a superior linearity in response (R^2 > 0.99) were realized for measuring of various green fluorescent reporters such as calcium indicators (Figure 9d) and flavin adenine dinucleotide (FAD) (Figure 9e).

5. CONCLUSIONS AND OUTLOOK

Bioelectronic interfaces integrating electrical and optical modalities represent unique tools to understand the brain and heart functions. In this context, transparent MEAs have become a versatile technology for simultaneous electrical and optical recording and modulation of cell activities at the cellular, tissue, and organ levels with high selectivity and spatiotemporal resolution. Compared to conventional opaque MEAs, the most important advantages of transparent MEAs are that they enable accurate colocalized electrical and optical investigations in a crosstalk-free manner without interfering with each other. This review first highlights recent advances in soft transparent microelectrode materials and structures that can be used as neural or cardiac interfaces. Next, a detailed summary of flexible and stretchable transparent MEA device designs, fabrication methods, and their applications on the brain and heart to understand the behaviors of neurons and cardiomyocytes, as well as to diagnose the health conditions and provide therapeutic benefits is introduced. Moreover, recent developments in constructing hybrid opto-electric devices with transparent microelectrodes, μ-LEDs, and/or μ-PDs for on-chip electrical and optical sensing and modulation are demonstrated. The representative characteristics of the transparent microelectrodes in Sections 3 and 4 are presented in Table 1.

Developing high-performance transparent microelectrodes that overcome the trade-off between microelectrode sizes, impedance, and optical transparency remains challenging. With further advances in materials, structural design, fabrication methods, transparent microelectrode-based soft electrical and opto-electric tools will open more opportunities in fundamental neuroscience and cardiology as well as enable innovative biomedical device development for treating neurological disorders and cardiovascular diseases. One natural evolution is to develop transparent conductors with additional functionalities such as neurochemical sensing.[141] In addition, there is an urgent need to design high density soft 2D or even 3D transparent microelectrode-based devices for probing a large volume of tissue on the surface or in the deep regions of organs with high spatiotemporal resolution and minimal invasiveness. In this context, devices with excellent biocompatibility, stretchable conformal mechanics, robust encapsulation, and substrate materials are crucial to realize stable chronic applications. Challenges in achieving superior mechanical performance for long-term use include the ability to maintain electrochemical sensing/stimulation performance and optical transparency during large mechanical strains/deformations and stretch/release cycles. In contrast, bioresorbable transparent microelectrodes that support implantable operations for a relatively short period of time and then disappear naturally over time afterward via bioresorption represent another direction of development to take advantage of the important benefits associated with bioresorbable electronics in promoting disease treatment (e.g., eliminating the needs for secondary surguries for device extraction).[142,143] Moreover, compared to conventional MEA technologies, scaling up the channel counts (thousands of channels) in transparent MEAs is more difficult, especially on soft substrates. Another milestone is to integrate a variety of components, such as light sources, photodetectors, optical filters, transparent microelectrodes, power sources, controls, data processing, and communication units together into wireless fully implantable devices for multimodal and/or closed-loop electrical and optical interrogation of organ functions with negligible adverse effects to the test subjects. Furthermore, integrating soft transparent microelectrodes into or onto existing biomedical devices could potentially facilitate diagnostics and treatments of diseases in clinical practices. For example, those transparent microelectrodes will allow for direct electrical sensing/stimulation and visualization of the underneath areas of interest to assist optical diagnostics/therapies or enhance tissue ablation efficiency when integrated on the tip of endoscopes.[144]

https://doi.org/10.1021/acsabm.3c00131
ACS Appl. Bio Mater. 2023, 6, 1701−1719

AUTHOR INFORMATION

Corresponding Author

Luyao Lu − *Department of Biomedical Engineering, The George Washington University, Washington, D.C. 20052, United States;* orcid.org/0000-0002-8784-2854; Email: luyaolu@gwu.edu

Complete contact information is available at: https://pubs.acs.org/10.1021/acsabm.3c00131

Notes

The author declares no competing financial interest.

ACKNOWLEDGMENTS

This work was finacially supported by National Science Foundation, Grants 2011093 and 2131682.

REFERENCES

(1) Choi, J. S.; Lee, H. J.; Rajaraman, S.; Kim, D.-H. Recent advances in three-dimensional microelectrode array technologies for in vitro and in vivo cardiac and neuronal interfaces. *Biosens. Bioelectron.* **2021**, *171*, 112687.

(2) Vázquez-Guardado, A.; Yang, Y.; Bandodkar, A. J.; Rogers, J. A. Recent advances in neurotechnologies with broad potential for neuroscience research. *Nat. Neurosci.* **2020**, *23*, 1522−1536.

(3) Liu, S.; Rao, Y.; Jang, H.; Tan, P.; Lu, N. Strategies for body-conformable electronics. *Matter* **2022**, *5*, 1104−1136.

(4) Hong, Y. J.; Jeong, H.; Cho, K. W.; Lu, N.; Kim, D.-H. Wearable and Implantable Devices for Cardiovascular Healthcare: from Monitoring to Therapy Based on Flexible and Stretchable Electronics. *Adv. Funct. Mater.* **2019**, *29*, 1808247.

(5) Jiang, Y.; Tian, B. Inorganic semiconductor biointerfaces. *Nat. Rev. Mater.* **2018**, *3*, 473−490.

(6) Spira, M. E.; Hai, A. Multi-electrode array technologies for neuroscience and cardiology. *Nat. Nanotechnol.* **2013**, *8*, 83−94.

(7) Shi, J.; Fang, Y. Flexible and Implantable Microelectrodes for Chronically Stable Neural Interfaces. *Adv. Mater.* **2019**, *31*, 1804895.

(8) Stett, A.; Egert, U.; Guenther, E.; Hofmann, F.; Meyer, T.; Nisch, W.; Haemmerle, H. Biological application of microelectrode arrays in drug discovery and basic research. *Anal. Bioanal. Chem.* **2003**, *377*, 486−495.

(9) Trohman, R. G.; Kim, M. H.; Pinski, S. L. Cardiac pacing: the state of the art. *Lancet* **2004**, *364*, 1701−1719.

(10) Cingolani, E.; Goldhaber, J. I.; Marbán, E. Next-generation pacemakers: from small devices to biological pacemakers. *Nat. Rev. Cardiol.* **2018**, *15*, 139−150.

(11) Dubrovskii, I. A.; Grigorov, S. S.; Bezzubchikov, V. A.; Vasil'ev, A. I. Implantable cardiac pacemakers. *Biomed. Eng.* **1976**, *10*, 335−340.

(12) Benabid, A. L.; Chabardes, S.; Mitrofanis, J.; Pollak, P. Deep brain stimulation of the subthalamic nucleus for the treatment of Parkinson's disease. *Lancet Neurol* **2009**, *8*, 67−81.

(13) Gardner, J. A history of deep brain stimulation: Technological innovation and the role of clinical assessment tools. *Soc. Stud. Sci.* **2013**, *43*, 707−728.

(14) Hong, G.; Lieber, C. M. Novel electrode technologies for neural recordings. *Nat. Rev. Neurosci.* **2019**, *20*, 330−345.

(15) Deisseroth, K. Optogenetics. *Nat. Methods* **2011**, *8*, 26−29.

(16) Entcheva, E.; Kay, M. W. Cardiac optogenetics: a decade of enlightenment. *Nat. Rev. Cardiol.* **2021**, *18*, 349−367.

(17) Häusser, M. Optogenetics: the age of light. *Nat. Methods* **2014**, *11*, 1012−1014.

(18) Rao, J.; Dragulescu-Andrasi, A.; Yao, H. Fluorescence imaging in vivo: recent advances. *Curr. Opin. Biotechnol.* **2007**, *18*, 17−25.

(19) Lin, M. Z.; Schnitzer, M. J. Genetically encoded indicators of neuronal activity. *Nat. Neurosci.* **2016**, *19*, 1142−1153.

(20) Yang, W.; Yuste, R. In vivo imaging of neural activity. *Nat. Methods* **2017**, *14*, 349−359.

(21) Wu, F.; Stark, E.; Ku, P.-C.; Wise, K. D.; Buzsaki, G.; Yoon, E. Monolithically Integrated μLEDs on Silicon Neural Probes for High-Resolution Optogenetic Studies in Behaving Animals. *Neuron* **2015**, *88*, 1136−1148.

(22) Ji, B.; Guo, Z.; Wang, M.; Yang, B.; Wang, X.; Li, W.; Liu, J. Flexible polyimide-based hybrid opto-electric neural interface with 16 channels of micro-LEDs and electrodes. *Microsyst. Nanoeng.* **2018**, *4*, 27.

(23) Obaid, S. N.; Chen, Z.; Lu, L. Advanced Electrical and Optical Microsystems for Biointerfacing. *Adv. Intell. Syst.* **2020**, *2*, 2000091.

(24) Kozai, T. D. Y.; Vazquez, A. L. Photoelectric artefact from optogenetics and imaging on microelectrodes and bioelectronics: new challenges and opportunities. *J. Mater. Chem. B* **2015**, *3*, 4965−4978.

(25) Park, D.-W.; Schendel, A. A.; Mikael, S.; Brodnick, S. K.; Richner, T. J.; Ness, J. P.; Hayat, M. R.; Atry, F.; Frye, S. T.; Pashaie, R.; Thongpang, S.; Ma, Z.; Williams, J. C. Graphene-based carbon-layered electrode array technology for neural imaging and optogenetic applications. *Nat. Commun.* **2014**, *5*, 5258.

(26) Kuzum, D.; Takano, H.; Shim, E.; Reed, J. C.; Juul, H.; Richardson, A. G.; de Vries, J.; Bink, H.; Dichter, M. A.; Lucas, T. H.; Coulter, D. A.; Cubukcu, E.; Litt, B. Transparent and flexible low noise graphene electrodes for simultaneous electrophysiology and neuroimaging. *Nat. Commun.* **2014**, *5*, 5259.

(27) Cho, Y. U.; Lee, J. Y.; Jeong, U.-J.; Park, S. H.; Lim, S. L.; Kim, K. Y.; Jang, J. W.; Park, J. H.; Kim, H. W.; Shin, H.; Jeon, H.; Jung, Y. M.; Cho, I.-J.; Yu, K. J. Ultra-Low Cost, Facile Fabrication of Transparent Neural Electrode Array for Electrocorticography with Photoelectric Artifact-Free Optogenetics. *Adv. Funct. Mater.* **2022**, *32*, 2105568.

(28) Chen, Z.; Boyajian, N.; Lin, Z.; Yin, R. T.; Obaid, S. N.; Tian, J.; Brennan, J. A.; Chen, S. W.; Miniovich, A. N.; Lin, L.; Qi, Y.; Liu, X.; Efimov, I. R.; Lu, L. Flexible and Transparent Metal Nanowire Microelectrode Arrays and Interconnects for Electrophysiology, Optogenetics, and Optical Mapping. *Adv. Mater. Technol.* **2021**, *6*, 2100225.

(29) Seo, J.-W.; Kim, K.; Seo, K.-W.; Kim, M. K.; Jeong, S.; Kim, H.; Ghim, J.-W.; Lee, J. H.; Choi, N.; Lee, J.-Y.; Lee, H. J. Artifact-Free 2D Mapping of Neural Activity In Vivo through Transparent Gold Nanonetwork Array. *Adv. Funct. Mater.* **2020**, *30*, 2000896.

(30) Seo, K. J.; Qiang, Y.; Bilgin, I.; Kar, S.; Vinegoni, C.; Weissleder, R.; Fang, H. Transparent Electrophysiology Microelectrodes and Interconnects from Metal Nanomesh. *ACS Nano* **2017**, *11*, 4365−4372.

(31) Qiang, Y.; Artoni, P.; Seo, K. J.; Culaclii, S.; Hogan, V.; Zhao, X.; Zhong, Y.; Han, X.; Wang, P.-M.; Lo, Y.-K.; Li, Y.; Patel, H. A.; Huang, Y.; Sambangi, A.; Chu, J. S. V.; Liu, W.; Fagiolini, M.; Fang, H. Transparent arrays of bilayer-nanomesh microelectrodes for simultaneous electrophysiology and two-photon imaging in the brain. *Sci. Adv.* **2018**, *4*, No. eaat0626.

(32) Kshirsagar, P.; Dickreuter, S.; Mierzejewski, M.; Burkhardt, C. J.; Chassé, T.; Fleischer, M.; Jones, P. D. Transparent Graphene/PEDOT:PSS Microelectrodes for Electro- and Optophysiology. *Adv. Mater. Technol.* **2019**, *4*, 1800318.

(33) Yang, W.; Gong, Y.; Yao, C.-Y.; Shrestha, M.; Jia, Y.; Qiu, Z.; Fan, Q. H.; Weber, A.; Li, W. A fully transparent, flexible PEDOT:PSS−ITO−Ag−ITO based microelectrode array for ECoG recording. *Lab Chip* **2021**, *21*, 1096−1108.

(34) Gao, X.; Liu, H.; Wang, D.; Zhang, J. Graphdiyne: synthesis, properties, and applications. *Chem. Soc. Rev.* **2019**, *48*, 908−936.

(35) VahidMohammadi, A.; Rosen, J.; Gogotsi, Y. The world of two-dimensional carbides and nitrides (MXenes). *Science* **2021**, *372*, No. eabf1581.

(36) Naguib, M.; Barsoum, M. W.; Gogotsi, Y. Ten Years of Progress in the Synthesis and Development of MXenes. *Adv. Mater.* **2021**, *33*, 2103393.

(37) Nair, R. R.; Blake, P.; Grigorenko, A. N.; Novoselov, K. S.; Booth, T. J.; Stauber, T.; Peres, N. M. R.; Geim, A. K. Fine Structure Constant Defines Visual Transparency of Graphene. *Science* **2008**, *320*, 1308.

(38) Chen, J.-H.; Jang, C.; Xiao, S.; Ishigami, M.; Fuhrer, M. S. Intrinsic and extrinsic performance limits of graphene devices on SiO_2. *Nat. Nanotechnol.* **2008**, *3*, 206−209.
(39) Park, D.-W.; Brodnick, S. K.; Ness, J. P.; Atry, F.; Krugner-Higby, L.; Sandberg, A.; Mikael, S.; Richner, T. J.; Novello, J.; Kim, H.; Baek, D.-H.; Bong, J.; Frye, S. T.; Thongpang, S.; Swanson, K. I.; Lake, W.; Pashaie, R.; Williams, J. C.; Ma, Z. Fabrication and utility of a transparent graphene neural electrode array for electrophysiology, in vivo imaging, and optogenetics. *Nat. Protoc.* **2016**, *11*, 2201−2222.
(40) Lee, C.; Wei, X.; Kysar, J. W.; Hone, J. Measurement of the Elastic Properties and Intrinsic Strength of Monolayer Graphene. *Science* **2008**, *321*, 385−388.
(41) Bolotin, K. I.; Sikes, K. J.; Jiang, Z.; Klima, M.; Fudenberg, G.; Hone, J.; Kim, P.; Stormer, H. L. Ultrahigh electron mobility in suspended graphene. *Solid State Commun.* **2008**, *146*, 351−355.
(42) De, S.; Coleman, J. N. Are There Fundamental Limitations on the Sheet Resistance and Transmittance of Thin Graphene Films? *ACS Nano* **2010**, *4*, 2713−2720.
(43) Park, S.-W.; Kim, J.; Kang, M.; Lee, W.; Park, B. S.; Kim, H.; Choi, S.-Y.; Yang, S.; Ahn, J.-H.; Yang, S. Epidural Electrotherapy for Epilepsy. *Small* **2018**, *14*, 1801732.
(44) Park, D.-W.; Ness, J. P.; Brodnick, S. K.; Esquibel, C.; Novello, J.; Atry, F.; Baek, D.-H.; Kim, H.; Bong, J.; Swanson, K. I.; Suminski, A. J.; Otto, K. J.; Pashaie, R.; Williams, J. C.; Ma, Z. Electrical Neural Stimulation and Simultaneous in Vivo Monitoring with Transparent Graphene Electrode Arrays Implanted in GCaMP6f Mice. *ACS Nano* **2018**, *12*, 148−157.
(45) Kabiri Ameri, S.; Ho, R.; Jang, H.; Tao, L.; Wang, Y.; Wang, L.; Schnyer, D. M.; Akinwande, D.; Lu, N. Graphene Electronic Tattoo Sensors. *ACS Nano* **2017**, *11*, 7634−7641.
(46) Heo, C.; Yoo, J.; Lee, S.; Jo, A.; Jung, S.; Yoo, H.; Lee, Y. H.; Suh, M. The control of neural cell-to-cell interactions through non-contact electrical field stimulation using graphene electrodes. *Biomaterials* **2011**, *32*, 19−27.
(47) Yin, R.; Xu, Z.; Mei, M.; Chen, Z.; Wang, K.; Liu, Y.; Tang, T.; Priydarshi, M. K.; Meng, X.; Zhao, S.; Deng, B.; Peng, H.; Liu, Z.; Duan, X. Soft transparent graphene contact lens electrodes for conformal full-cornea recording of electroretinogram. *Nat. Commun.* **2018**, *9*, 2334.
(48) Savchenko, A.; Cherkas, V.; Liu, C.; Braun, G. B.; Kleschevnikov, A.; Miller, Y. I.; Molokanova, E. Graphene biointerfaces for optical stimulation of cells. *Sci. Adv.* **2018**, *4*, No. eaat0351.
(49) Chen, C.-H.; Lin, C.-T.; Hsu, W.-L.; Chang, Y.-C.; Yeh, S.-R.; Li, L.-J.; Yao, D.-J. A flexible hydrophilic-modified graphene microprobe for neural and cardiac recording. *Nanomed.: Nanotechnol. Biol. Med.* **2013**, *9*, 600−604.
(50) Lu, Y.; Lyu, H.; Richardson, A. G.; Lucas, T. H.; Kuzum, D. Flexible Neural Electrode Array Based-on Porous Graphene for Cortical Microstimulation and Sensing. *Sci. Rep.* **2016**, *6*, 33526.
(51) Wang, K.; Frewin, C. L.; Esrafilzadeh, D.; Yu, C.; Wang, C.; Pancrazio, J. J.; Romero-Ortega, M.; Jalili, R.; Wallace, G. High-Performance Graphene-Fiber-Based Neural Recording Microelectrodes. *Adv. Mater.* **2019**, *31*, 1805867.
(52) Lu, Y.; Liu, X.; Hattori, R.; Ren, C.; Zhang, X.; Komiyama, T.; Kuzum, D. Ultralow Impedance Graphene Microelectrodes with High Optical Transparency for Simultaneous Deep Two-Photon Imaging in Transgenic Mice. *Adv. Funct. Mater.* **2018**, *28*, 1800002.
(53) Schnorr, J. M.; Swager, T. M. Emerging Applications of Carbon Nanotubes. *Chem. Mater.* **2011**, *23*, 646−657.
(54) McCoul, D.; Hu, W.; Gao, M.; Mehta, V.; Pei, Q. Recent Advances in Stretchable and Transparent Electronic Materials. *Adv. Electron. Mater.* **2016**, *2*, 1500407.
(55) Pereira, L. F. C.; Rocha, C. G.; Latgé, A.; Coleman, J. N.; Ferreira, M. S. Upper bound for the conductivity of nanotube networks. *Appl. Phys. Lett.* **2009**, *95*, 123106.
(56) Wang, C. Y.; Zhang, L. C. A critical assessment of the elastic properties and effective wall thickness of single-walled carbon nanotubes. *Nanotechnology* **2008**, *19*, 075705.
(57) Schreiber, M.; Lutz, T.; Keeley, G. P.; Kumar, S.; Boese, M.; Krishnamurthy, S.; Duesberg, G. S. Transparent ultrathin conducting carbon films. *Appl. Surf. Sci.* **2010**, *256*, 6186−6190.
(58) Li, Z.; Kandel, H. R.; Dervishi, E.; Saini, V.; Biris, A. S.; Biris, A. R.; Lupu, D. Does the wall number of carbon nanotubes matter as conductive transparent material? *Appl. Phys. Lett.* **2007**, *91*, 053115.
(59) Biswas, C.; Lee, Y. H. Graphene Versus Carbon Nanotubes in Electronic Devices. *Adv. Funct. Mater.* **2011**, *21*, 3806−3826.
(60) Wong, E. W.; Sheehan, P. E.; Lieber, C. M. Nanobeam Mechanics: Elasticity, Strength, and Toughness of Nanorods and Nanotubes. *Science* **1997**, *277*, 1971−1975.
(61) Li, Z.; Jia, Y.; Wei, J.; Wang, K.; Shu, Q.; Gui, X.; Zhu, H.; Cao, A.; Wu, D. Large area, highly transparent carbon nanotube spiderwebs for energy harvesting. *J. Mater. Chem.* **2010**, *20*, 7236−7240.
(62) Wu, Z.; Chen, Z.; Du, X.; Logan, J. M.; Sippel, J.; Nikolou, M.; Kamaras, K.; Reynolds, J. R.; Tanner, D. B.; Hebard, A. F.; Rinzler, A. G. Transparent, Conductive Carbon Nanotube Films. *Science* **2004**, *305*, 1273−1276.
(63) Arash, B.; Wang, Q.; Varadan, V. K. Mechanical properties of carbon nanotube/polymer composites. *Sci. Rep.* **2014**, *4*, 6479.
(64) Zhang, Y.; Li, Z.; Li, H.; Gao, J.; Zhang, J.; Zeng, Y. Effect of carbon nanotubes shape on the properties of multiwall carbon nanotubes/polyethylene flexible transparent conductive films. *J. Mater. Sci. Mater. Electron.* **2014**, *25*, 2692−2696.
(65) Bianco, A.; Kostarelos, K.; Prato, M. Making carbon nanotubes biocompatible and biodegradable. *Chem. Commun.* **2011**, *47*, 10182−10188.
(66) Schipper, M. L.; Nakayama-Ratchford, N.; Davis, C. R.; Kam, N. W. S.; Chu, P.; Liu, Z.; Sun, X.; Dai, H.; Gambhir, S. S. A pilot toxicology study of single-walled carbon nanotubes in a small sample of mice. *Nat. Nanotechnol.* **2008**, *3*, 216−221.
(67) Angelini, G.; Boncompagni, S.; De Maria, P.; De Nardi, M.; Fontana, A.; Gasbarri, C.; Menna, E. Layer-by-layer deposition of shortened nanotubes or polyethylene glycol-derivatized nanotubes on liposomes: A tool for increasing liposome stability. *Carbon* **2007**, *45*, 2479−2485.
(68) Lovat, V.; Pantarotto, D.; Lagostena, L.; Cacciari, B.; Grandolfo, M.; Righi, M.; Spalluto, G.; Prato, M.; Ballerini, L. Carbon Nanotube Substrates Boost Neuronal Electrical Signaling. *Nano Lett.* **2005**, *5*, 1107−1110.
(69) Keefer, E. W.; Botterman, B. R.; Romero, M. I.; Rossi, A. F.; Gross, G. W. Carbon nanotube coating improves neuronal recordings. *Nat. Nanotechnol.* **2008**, *3*, 434−439.
(70) Cellot, G.; Cilia, E.; Cipollone, S.; Rancic, V.; Sucapane, A.; Giordani, S.; Gambazzi, L.; Markram, H.; Grandolfo, M.; Scaini, D.; Gelain, F.; Casalis, L.; Prato, M.; Giugliano, M.; Ballerini, L. Carbon nanotubes might improve neuronal performance by favouring electrical shortcuts. *Nat. Nanotechnol.* **2009**, *4*, 126−133.
(71) Su, H.-C.; Lin, C.-M.; Yen, S.-J.; Chen, Y.-C.; Chen, C.-H.; Yeh, S.-R.; Fang, W.; Chen, H.; Yao, D.-J.; Chang, Y.-C.; Yew, T.-R. A cone-shaped 3D carbon nanotube probe for neural recording. *Biosens. Bioelectron.* **2010**, *26*, 220−227.
(72) Chen, Y.-C.; Hsu, H.-L.; Lee, Y.-T.; Su, H.-C.; Yen, S.-J.; Chen, C.-H.; Hsu, W.-L.; Yew, T.-R.; Yeh, S.-R.; Yao, D.-J.; Chang, Y.-C.; Chen, H. An active, flexible carbon nanotube microelectrode array for recording electrocorticograms. *J. Neural Eng.* **2011**, *8*, 034001.
(73) Rivnay, J.; Inal, S.; Collins, B. A.; Sessolo, M.; Stavrinidou, E.; Strakosas, X.; Tassone, C.; Delongchamp, D. M.; Malliaras, G. G. Structural control of mixed ionic and electronic transport in conducting polymers. *Nat. Commun.* **2016**, *7*, 11287.
(74) Jastrzebska-Perfect, P.; Spyropoulos, G. D.; Cea, C.; Zhao, Z.; Rauhala, O. J.; Viswanathan, A.; Sheth, S. A.; Gelinas, J. N.; Khodagholy, D. Mixed-conducting particulate composites for soft electronics. *Sci. Adv.* **2020**, *6*, No. eaaz6767.
(75) Green, R.; Abidian, M. R. Conducting Polymers for Neural Prosthetic and Neural Interface Applications. *Adv. Mater.* **2015**, *27*, 7620−7637.

https://doi.org/10.1021/acsabm.3c00131
ACS Appl. Bio Mater. 2023, 6, 1701−1719

(76) Simon, D. T.; Gabrielsson, E. O.; Tybrandt, K.; Berggren, M. Organic Bioelectronics: Bridging the Signaling Gap between Biology and Technology. *Chem. Rev.* **2016**, *116*, 13009−13041.
(77) Zhan, C.; Yu, G.; Lu, Y.; Wang, L.; Wujcik, E.; Wei, S. Conductive polymer nanocomposites: a critical review of modern advanced devices. *J. Mater. Chem. C* **2017**, *5*, 1569−1585.
(78) Bettucci, O.; Matrone, G. M.; Santoro, F. Conductive Polymer-Based Bioelectronic Platforms toward Sustainable and Biointegrated Devices: A Journey from Skin to Brain across Human Body Interfaces. *Adv. Mater. Technol.* **2022**, *7*, 2100293.
(79) Pranti, A. S.; Schander, A.; Bödecker, A.; Lang, W. PEDOT: PSS coating on gold microelectrodes with excellent stability and high charge injection capacity for chronic neural interfaces. *Sens. Actuators B Chem.* **2018**, *275*, 382−393.
(80) Wang, A.; Jung, D.; Lee, D.; Wang, H. Impedance Characterization and Modeling of Subcellular to Micro-sized Electrodes with Varying Materials and PEDOT:PSS Coating for Bioelectrical Interfaces. *ACS Appl. Electron. Mater.* **2021**, *3*, 5226−5239.
(81) Li, Q.; Nan, K.; Le Floch, P.; Lin, Z.; Sheng, H.; Blum, T. S.; Liu, J. Cyborg Organoids: Implantation of Nanoelectronics via Organogenesis for Tissue-Wide Electrophysiology. *Nano Lett.* **2019**, *19*, 5781−5789.
(82) Han, L.; Yan, L.; Wang, M.; Wang, K.; Fang, L.; Zhou, J.; Fang, J.; Ren, F.; Lu, X. Transparent, Adhesive, and Conductive Hydrogel for Soft Bioelectronics Based on Light-Transmitting Polydopamine-Doped Polypyrrole Nanofibrils. *Chem. Mater.* **2018**, *30*, 5561−5572.
(83) Cui, X.; Lee, V. A.; Raphael, Y.; Wiler, J. A.; Hetke, J. F.; Anderson, D. J.; Martin, D. C. Surface modification of neural recording electrodes with conducting polymer/biomolecule blends. *J. Biomed. Mater. Res.* **2001**, *56*, 261−272.
(84) Wang, Z.; Cui, H.; Li, S.; Feng, X.; Aghassi-Hagmann, J.; Azizian, S.; Levkin, P. A. Facile Approach to Conductive Polymer Microelectrodes for Flexible Electronics. *ACS Appl. Mater. Interfaces* **2021**, *13*, 21661−21668.
(85) Blau, A.; Murr, A.; Wolff, S.; Sernagor, E.; Medini, P.; Iurilli, G.; Ziegler, C.; Benfenati, F. Flexible, all-polymer microelectrode arrays for the capture of cardiac and neuronal signals. *Biomaterials* **2011**, *32*, 1778−1786.
(86) Sessolo, M.; Khodagholy, D.; Rivnay, J.; Maddalena, F.; Gleyzes, M.; Steidl, E.; Buisson, B.; Malliaras, G. G. Easy-to-Fabricate Conducting Polymer Microelectrode Arrays. *Adv. Mater.* **2013**, *25*, 2135−2139.
(87) Guo, L.; Ma, M.; Zhang, N.; Langer, R.; Anderson, D. G. Stretchable Polymeric Multielectrode Array for Conformal Neural Interfacing. *Adv. Mater.* **2014**, *26*, 1427−1433.
(88) Qi, D.; Liu, Z.; Liu, Y.; Jiang, Y.; Leow, W. R.; Pal, M.; Pan, S.; Yang, H.; Wang, Y.; Zhang, X.; Yu, J.; Li, B.; Yu, Z.; Wang, W.; Chen, X. Highly Stretchable, Compliant, Polymeric Microelectrode Arrays for In Vivo Electrophysiological Interfacing. *Adv. Mater.* **2017**, *29*, 1702800.
(89) Kim, N.; Kee, S.; Lee, S. H.; Lee, B. H.; Kahng, Y. H.; Jo, Y.-R.; Kim, B.-J.; Lee, K. Highly Conductive PEDOT:PSS Nanofibrils Induced by Solution-Processed Crystallization. *Adv. Mater.* **2014**, *26*, 2268−2272.
(90) Singh, R.; Tharion, J.; Murugan, S.; Kumar, A. ITO-Free Solution-Processed Flexible Electrochromic Devices Based on PEDOT:PSS as Transparent Conducting Electrode. *ACS Appl. Mater. Interfaces* **2017**, *9*, 19427−19435.
(91) Dijk, G.; Kaszas, A.; Pas, J.; O'Connor, R. P. Fabrication and in vivo 2-photon microscopy validation of transparent PEDOT:PSS microelectrode arrays. *Microsyst. Nanoeng.* **2022**, *8*, 90.
(92) Wan, A. M.-D.; Inal, S.; Williams, T.; Wang, K.; Leleux, P.; Estevez, L.; Giannelis, E. P.; Fischbach, C.; Malliaras, G. G.; Gourdon, D. 3D conducting polymer platforms for electrical control of protein conformation and cellular functions. *J. Mater. Chem. B* **2015**, *3*, 5040−5048.
(93) Sasaki, M.; Karikkineth, B. C.; Nagamine, K.; Kaji, H.; Torimitsu, K.; Nishizawa, M. Highly Conductive Stretchable and Biocompatible Electrode−Hydrogel Hybrids for Advanced Tissue Engineering. *Adv. Healthc. Mater.* **2014**, *3*, 1919−1927.
(94) Susloparova, A.; Halliez, S.; Begard, S.; Colin, M.; Buée, L.; Pecqueur, S.; Alibart, F.; Thomy, V.; Arscott, S.; Pallecchi, E.; Coffinier, Y. Low impedance and highly transparent microelectrode arrays (MEA) for in vitro neuron electrical activity probing. *Sens. Actuators B Chem.* **2021**, *327*, 128895.
(95) Wang, Y.; Zhu, C.; Pfattner, R.; Yan, H.; Jin, L.; Chen, S.; Molina-Lopez, F.; Lissel, F.; Liu, J.; Rabiah, N. I.; Chen, Z.; Chung, J. W.; Linder, C.; Toney, M. F.; Murmann, B.; Bao, Z. A highly stretchable, transparent, and conductive polymer. *Sci. Adv.* **2017**, *3*, No. e1602076.
(96) Vosgueritchian, M.; Lipomi, D. J.; Bao, Z. Highly Conductive and Transparent PEDOT:PSS Films with a Fluorosurfactant for Stretchable and Flexible Transparent Electrodes. *Adv. Funct. Mater.* **2012**, *22*, 421−428.
(97) Savagatrup, S.; Chan, E.; Renteria-Garcia, S. M.; Printz, A. D.; Zaretski, A. V.; O'Connor, T. F.; Rodriquez, D.; Valle, E.; Lipomi, D. J. Plasticization of PEDOT:PSS by Common Additives for Mechanically Robust Organic Solar Cells and Wearable Sensors. *Adv. Funct. Mater.* **2015**, *25*, 427−436.
(98) Oh, J. Y.; Kim, S.; Baik, H.-K.; Jeong, U. Conducting Polymer Dough for Deformable Electronics. *Adv. Mater.* **2016**, *28*, 4455−4461.
(99) Donaldson, P. D.; Swisher, S. L. Transparent, Low-Impedance Inkjet-Printed PEDOT:PSS Microelectrodes for Multimodal Neuroscience. *Phys. Status Solidi* **2022**, *219*, 2100683.
(100) Miller, M. S.; O'Kane, J. C.; Niec, A.; Carmichael, R. S.; Carmichael, T. B. Silver Nanowire/Optical Adhesive Coatings as Transparent Electrodes for Flexible Electronics. *ACS Appl. Mater. Interfaces* **2013**, *5*, 10165−10172.
(101) Bid, A.; Bora, A.; Raychaudhuri, A. K. Temperature dependence of the resistance of metallic nanowires of diameter ≥ 15 nm: Applicability of Bloch-Grüneisen theorem. *Phys. Rev. B* **2006**, *74*, 035426.
(102) Coskun, S.; Selen Ates, E.; Emrah Unalan, H. Optimization of silver nanowire networks for polymer light emitting diode electrodes. *Nanotechnology* **2013**, *24*, 125202.
(103) Langley, D. P.; Lagrange, M.; Giusti, G.; Jiménez, C.; Bréchet, Y.; Nguyen, N. D.; Bellet, D. Metallic nanowire networks: effects of thermal annealing on electrical resistance. *Nanoscale* **2014**, *6*, 13535−13543.
(104) Tokuno, T.; Nogi, M.; Karakawa, M.; Jiu, J.; Nge, T. T.; Aso, Y.; Suganuma, K. Fabrication of silver nanowire transparent electrodes at room temperature. *Nano Res.* **2011**, *4*, 1215−1222.
(105) Stewart, I. E.; Rathmell, A. R.; Yan, L.; Ye, S.; Flowers, P. F.; You, W.; Wiley, B. J. Solution-processed copper−nickel nanowire anodes for organic solar cells. *Nanoscale* **2014**, *6*, 5980−5988.
(106) Lee, J.; Lee, P.; Lee, H.; Lee, D.; Lee, S. S.; Ko, S. H. Very long Ag nanowire synthesis and its application in a highly transparent, conductive and flexible metal electrode touch panel. *Nanoscale* **2012**, *4*, 6408−6414.
(107) Choi, S.; Han, S. I.; Jung, D.; Hwang, H. J.; Lim, C.; Bae, S.; Park, O. K.; Tschabrunn, C. M.; Lee, M.; Bae, S. Y.; Yu, J. W.; Ryu, J. H.; Lee, S.-W.; Park, K.; Kang, P. M.; Lee, W. B.; Nezafat, R.; Hyeon, T.; Kim, D.-H. Highly conductive, stretchable and biocompatible Ag−Au core−sheath nanowire composite for wearable and implantable bioelectronics. *Nat. Nanotechnol.* **2018**, *13*, 1048−1056.
(108) Chen, Z.; Nguyen, K.; Kowalik, G.; Shi, X.; Tian, J.; Doshi, M.; Alber, B. R.; Guan, X.; Liu, X.; Ning, X.; Kay, M. W.; Lu, L. Transparent and stretchable Au-Ag nanowire recording microelectrode arrays. *Adv. Mater. Technol.* **2023**, 2201716.
(109) Obaid, S. N.; Yin, R. T.; Tian, J.; Chen, Z.; Chen, S. W.; Lee, K. B.; Boyajian, N.; Miniovich, A. N.; Efimov, I. R.; Lu, L. Multifunctional Flexible Biointerfaces for Simultaneous Colocalized Optophysiology and Electrophysiology. *Adv. Funct. Mater.* **2020**, *30*, 1910027.
(110) Khan, A.; Liang, C.; Huang, Y.-T.; Zhang, C.; Cai, J.; Feng, S.-P.; Li, W.-D. Template-Electrodeposited and Imprint-Transferred Microscale Metal-Mesh Transparent Electrodes for Flexible and Stretchable Electronics. *Adv. Eng. Mater.* **2019**, *21*, 1900723.
(111) Schneider, J.; Rohner, P.; Thureja, D.; Schmid, M.; Galliker, P.; Poulikakos, D. Electrohydrodynamic NanoDrip Printing of High

https://doi.org/10.1021/acsabm.3c00131
ACS Appl. Bio Mater. 2023, 6, 1701−1719

Aspect Ratio Metal Grid Transparent Electrodes. *Adv. Funct. Mater.* **2016**, *26*, 833−840.
(112) Hong, S.; Yeo, J.; Kim, G.; Kim, D.; Lee, H.; Kwon, J.; Lee, H.; Lee, P.; Ko, S. H. Nonvacuum, Maskless Fabrication of a Flexible Metal Grid Transparent Conductor by Low-Temperature Selective Laser Sintering of Nanoparticle Ink. *ACS Nano* **2013**, *7*, 5024−5031.
(113) Park, J. H.; Lee, D. Y.; Kim, Y.-H.; Kim, J. K.; Lee, J. H.; Park, J. H.; Lee, T.-W.; Cho, J. H. Flexible and Transparent Metallic Grid Electrodes Prepared by Evaporative Assembly. *ACS Appl. Mater. Interfaces* **2014**, *6*, 12380−12387.
(114) Jung, S.; Lee, S.; Song, M.; Kim, D.-G.; You, D. S.; Kim, J.-K.; Kim, C. S.; Kim, T.-M.; Kim, K.-H.; Kim, J.-J.; Kang, J.-W. Extremely Flexible Transparent Conducting Electrodes for Organic Devices. *Adv. Energy Mater.* **2014**, *4*, 1300474.
(115) Qiang, Y.; Seo, K. J.; Zhao, X.; Artoni, P.; Golshan, N. H.; Culaclii, S.; Wang, P.-M.; Liu, W.; Ziemer, K. S.; Fagiolini, M.; Fang, H. Bilayer Nanomesh Structures for Transparent Recording and Stimulating Microelectrodes. *Adv. Funct. Mater.* **2017**, *27*, 1704117.
(116) Chen, Z.; Yin, R. T.; Obaid, S. N.; Tian, J.; Chen, S. W.; Miniovich, A. N.; Boyajian, N.; Efimov, I. R.; Lu, L. Flexible and Transparent Metal Oxide/Metal Grid Hybrid Interfaces for Electrophysiology and Optogenetics. *Adv. Mater. Technol.* **2020**, *5*, 2000322.
(117) Guo, C. F.; Sun, T.; Liu, Q.; Suo, Z.; Ren, Z. Highly stretchable and transparent nanomesh electrodes made by grain boundary lithography. *Nat. Commun.* **2014**, *5*, 3121.
(118) Jin, W.-Y.; Ginting, R. T.; Ko, K.-J.; Kang, J.-W. Ultra-Smooth, Fully Solution-Processed Large-Area Transparent Conducting Electrodes for Organic Devices. *Sci. Rep.* **2016**, *6*, 36475.
(119) Whyte, W.; Roche, E. T.; Varela, C. E.; Mendez, K.; Islam, S.; O'Neill, H.; Weafer, F.; Shirazi, R. N.; Weaver, J. C.; Vasilyev, N. V.; McHugh, P. E.; Murphy, B.; Duffy, G. P.; Walsh, C. J.; Mooney, D. J. Sustained release of targeted cardiac therapy with a replenishable implanted epicardial reservoir. *Nat. Biomed. Eng.* **2018**, *2*, 416−428.
(120) Thunemann, M.; Lu, Y.; Liu, X.; Kılıç, K.; Desjardins, M.; Vandenberghe, M.; Sadegh, S.; Saisan, P. A.; Cheng, Q.; Weldy, K. L.; Lyu, H.; Djurovic, S.; Andreassen, O. A.; Dale, A. M.; Devor, A.; Kuzum, D. Deep 2-photon imaging and artifact-free optogenetics through transparent graphene microelectrode arrays. *Nat. Commun.* **2018**, *9*, 2035.
(121) Driscoll, N.; Rosch, R. E.; Murphy, B. B.; Ashourvan, A.; Vishnubhotla, R.; Dickens, O. O.; Johnson, A. T. C.; Davis, K. A.; Litt, B.; Bassett, D. S.; Takano, H.; Vitale, F. Multimodal in vivo recording using transparent graphene microelectrodes illuminates spatiotemporal seizure dynamics at the microscale. *Commun. Biol.* **2021**, *4*, 136.
(122) Donaldson, P. D.; Navabi, Z. S.; Carter, R. E.; Fausner, S. M. L.; Ghanbari, L.; Ebner, T. J.; Swisher, S. L.; Kodandaramaiah, S. B. Polymer Skulls With Integrated Transparent Electrode Arrays for Cortex-Wide Opto-Electrophysiological Recordings. *Adv. Healthc. Mater.* **2022**, *11*, 2200626.
(123) Viventi, J.; Kim, D.-H.; Vigeland, L.; Frechette, E. S.; Blanco, J. A.; Kim, Y.-S.; Avrin, A. E.; Tiruvadi, V. R.; Hwang, S.-W.; Vanleer, A. C.; Wulsin, D. F.; Davis, K.; Gelber, C. E.; Palmer, L.; Van der Spiegel, J.; Wu, J.; Xiao, J.; Huang, Y.; Contreras, D.; Rogers, J. A.; Litt, B. Flexible, foldable, actively multiplexed, high-density electrode array for mapping brain activity in vivo. *Nat. Neurosci.* **2011**, *14*, 1599−1605.
(124) Lee, W.; Someya, T. Emerging Trends in Flexible Active Multielectrode Arrays. *Chem. Mater.* **2019**, *31*, 6347−6358.
(125) Lee, W.; Kim, D.; Matsuhisa, N.; Nagase, M.; Sekino, M.; Malliaras, G. G.; Yokota, T.; Someya, T. Transparent, conformable, active multielectrode array using organic electrochemical transistors. *Proc. Natl. Acad. Sci. U.S.A.* **2017**, *114*, 10554−10559.
(126) Takemoto, A.; Araki, T.; Nishimura, K.; Akiyama, M.; Uemura, T.; Kiriyama, K.; Koot, J. M.; Kasai, Y.; Kurihira, N.; Osaki, S.; Wakida, S.-i.; den Toonder, J. M. J.; Sekitani, T. Fully Transparent, Ultrathin Flexible Organic Electrochemical Transistors with Additive Integration for Bioelectronic Applications. *Adv. Sci.* **2023**, *10*, 2204746.
(127) Park, J.; Choi, S.; Janardhan, A. H.; Lee, S.-Y.; Raut, S.; Soares, J.; Shin, K.; Yang, S.; Lee, C.; Kang, K.-W.; Cho, H. R.; Kim, S. J.; Seo, P.; Hyun, W.; Jung, S.; Lee, H.-J.; Lee, N.; Choi, S. H.; Sacks, M.; Lu, N.; Josephson, M. E.; Hyeon, T.; Kim, D.-H.; Hwang, H. J. Electromechanical cardioplasty using a wrapped elasto-conductive epicardial mesh. *Sci. Transl. Med.* **2016**, *8*, 344ra86.
(128) Zhang, J.; Liu, X.; Xu, W.; Luo, W.; Li, M.; Chu, F.; Xu, L.; Cao, A.; Guan, J.; Tang, S.; Duan, X. Stretchable Transparent Electrode Arrays for Simultaneous Electrical and Optical Interrogation of Neural Circuits in Vivo. *Nano Lett.* **2018**, *18*, 2903−2911.
(129) Renz, A. F.; Lee, J.; Tybrandt, K.; Brzezinski, M.; Lorenzo, D. A.; Cerra Cheraka, M.; Lee, J.; Helmchen, F.; Vörös, J.; Lewis, C. M. Opto-E-Dura: A Soft, Stretchable ECoG Array for Multimodal, Multiscale Neuroscience. *Adv. Healthc. Mater.* **2020**, *9*, 2000814.
(130) Lee, J.; Ozden, I.; Song, Y.-K.; Nurmikko, A. V. Transparent intracortical microprobe array for simultaneous spatiotemporal optical stimulation and multichannel electrical recording. *Nat. Methods* **2015**, *12*, 1157−1162.
(131) Seo, K. J.; Artoni, P.; Qiang, Y.; Zhong, Y.; Han, X.; Shi, Z.; Yao, W.; Fagiolini, M.; Fang, H. Transparent, Flexible, Penetrating Microelectrode Arrays with Capabilities of Single-Unit Electrophysiology. *Adv. Biosyst.* **2019**, *3*, 1800276.
(132) Finegold, J. A.; Asaria, P.; Francis, D. P. Mortality from ischaemic heart disease by country, region, and age: Statistics from World Health Organisation and United Nations. *Int. J. Cardiol.* **2013**, *168*, 934−945.
(133) Gaziano, T. A.; Bitton, A.; Anand, S.; Abrahams-Gessel, S.; Murphy, A. Growing Epidemic of Coronary Heart Disease in Low- and Middle-Income Countries. *Curr. Probl. Cardiol.* **2010**, *35*, 72−115.
(134) Tian, J.; Lin, Z.; Chen, Z.; Obaid, S. N.; Efimov, I. R.; Lu, L. Stretchable and Transparent Metal Nanowire Microelectrodes for Simultaneous Electrophysiology and Optogenetics Applications. *Photonics* **2021**, *8*, 220.
(135) Pan, T.; Pharr, M.; Ma, Y.; Ning, R.; Yan, Z.; Xu, R.; Feng, X.; Huang, Y.; Rogers, J. A. Experimental and Theoretical Studies of Serpentine Interconnects on Ultrathin Elastomers for Stretchable Electronics. *Adv. Funct. Mater.* **2017**, *27*, 1702589.
(136) Kwon, K. Y.; Sirowatka, B.; Weber, A.; Li, W. Opto-μECoG Array: A Hybrid Neural Interface With Transparent μECoG Electrode Array and Integrated LEDs for Optogenetics. *IEEE Trans. Biomed. Circuits Syst.* **2013**, *7*, 593−600.
(137) Kim, T.-i.; McCall, J. G.; Jung, Y. H.; Huang, X.; Siuda, E. R.; Li, Y.; Song, J.; Song, Y. M.; Pao, H. A.; Kim, R.-H.; Lu, C.; Lee, S. D.; Song, I.-S.; Shin, G.; Al-Hasani, R.; Kim, S.; Tan, M. P.; Huang, Y.; Omenetto, F. G.; Rogers, J. A.; Bruchas, M. R. Injectable, Cellular-Scale Optoelectronics with Applications for Wireless Optogenetics. *Science* **2013**, *340*, 211−216.
(138) Park, J.; Bong, J.; Jung, Y. H.; Kegel, J.; Liu, B.; Suminski, A. J.; Brodnick, S. K.; Jang, H.; Yu, Z.; Williams, J. C.; Ma, Z. Design and Fabrication of Blue LED-Integrated Graphene Electrodes for Neural Stimulation and Signal Recording. *ACS Appl. Electron. Mater.* **2021**, *3*, 4308−4316.
(139) Obaid, S. N.; Chen, Z.; Madrid, M.; Lin, Z.; Tian, J.; Humphreys, C.; Adams, J.; Daza, N.; Balansag, J.; Efimov, I. R.; Lu, L. Flexible Electro-Optical Arrays for Simultaneous Multi-Site Colocalized Spatiotemporal Cardiac Mapping and Modulation. *Adv. Opt. Mater.* **2022**, *10*, 2201331.
(140) Obaid, S. N.; Quirion, N.; Torres Balansag, J. D.; Daza, N.; Shi, X.; Chen, Z.; Lu, L. Design and Fabrication of a Flexible Opto-Electric Biointerface for Multimodal Optical Fluorescence and Electrical Recording. *ACS Appl. Electron. Mater.* **2023**, *5*, 1688−1696.
(141) Liu, C.; Zhao, Y.; Cai, X.; Xie, Y.; Wang, T.; Cheng, D.; Li, L.; Li, R.; Deng, Y.; Ding, H.; Lv, G.; Zhao, G.; Liu, L.; Zou, G.; Feng, M.; Sun, Q.; Yin, L.; Sheng, X. A wireless, implantable optoelectrochemical probe for optogenetic stimulation and dopamine detection. *Microsyst. Nanoeng.* **2020**, *6*, 64.
(142) Kang, S.-K.; Koo, J.; Lee, Y. K.; Rogers, J. A. Advanced Materials and Devices for Bioresorbable Electronics. *Acc. Chem. Res.* **2018**, *51*, 988−998.
(143) Choi, Y. S.; Yin, R. T.; Pfenniger, A.; Koo, J.; Avila, R.; Benjamin Lee, K.; Chen, S. W.; Lee, G.; Li, G.; Qiao, Y.; Murillo-Berlioz, A.; Kiss, A.; Han, S.; Lee, S. M.; Li, C.; Xie, Z.; Chen, Y.-Y.; Burrell, A.; Geist, B.;

https://doi.org/10.1021/acsabm.3c00131
ACS Appl. Bio Mater. 2023, 6, 1701−1719

Jeong, H.; Kim, J.; Yoon, H.-J.; Banks, A.; Kang, S.-K.; Zhang, Z. J.; Haney, C. R.; Sahakian, A. V.; Johnson, D.; Efimova, T.; Huang, Y.; Trachiotis, G. D.; Knight, B. P.; Arora, R. K.; Efimov, I. R.; Rogers, J. A. Fully implantable and bioresorbable cardiac pacemakers without leads or batteries. *Nat. Biotechnol.* **2021**, *39*, 1228−1238.

(144) Nguyen, T.-K.; Yadav, S.; Truong, T.-A.; Han, M.; Barton, M.; Leitch, M.; Guzman, P.; Dinh, T.; Ashok, A.; Vu, H.; Dau, V.; Haasmann, D.; Chen, L.; Park, Y.; Do, T. N.; Yamauchi, Y.; Rogers, J. A.; Nguyen, N.-T.; Phan, H.-P. Integrated, Transparent Silicon Carbide Electronics and Sensors for Radio Frequency Biomedical Therapy. *ACS Nano* **2022**, *16*, 10890−10903.

https://doi.org/10.1021/acsabm.3c00131
ACS Appl. Bio Mater. 2023, 6, 1701−1719